J. Fluid Mech. (2013), *vol.* 737, *pp.* 466–498.
doi:10.1017/jfm.2013.553

Organized large structure in the post-transition mixing layer. Part 1. Experimental evidence

A. D'Ovidio and C. M. Coats†

Department of Engineering, University of Leicester, Leicester LE1 7RH, UK

(Received 23 August 2012; revised 11 June 2013; accepted 11 October 2013;
first published online 26 November 2013)

New flow-visualization experiments on mixing layers of various velocity and density ratios are reported. It is shown that, in mixing layers developing from laminar initial conditions, the familiar mechanism of growth by vortex amalgamation is replaced at the mixing transition by a previously unrecognized mechanism in which the spanwise-coherent large structures individually undergo continuous linear growth. In the organized post-transition flow it is this continuous linear growth of the individual structures that produces the self-similar growth of the mixing-layer thickness, with the occasional interactions between neighbouring structures occurring as a consequence of their growth, not its cause. It is also observed that periods during which the post-transition mixing layer comprises orderly processions of large structures alternate with periods during which no large-scale organization is apparent downstream of the transition location. These two fully turbulent flow states are characterized by different growth rates, entrainment ratios and orientations of the mixing layer relative to the free streams. The implications of these findings are discussed.

Key words: free shear layers, shear layer turbulence, turbulent transition

1. Introduction

In its fully developed state the plane turbulent mixing layer is, according to classical turbulence theory (Townsend 1976), a self-preserving turbulent flow which is in a state of dynamic equilibrium and whose growth rate is a function only of the velocity and density ratios between the free streams. As was discussed in this journal by Brown & Roshko (1974), it was therefore an unsatisfactory situation that careful measurements made for the same free-stream conditions in different wind tunnels had yielded apparently self-similar mixing-layer growth rates which varied very significantly. Wygnanski & Fiedler (1970), for example, had obtained a growth rate for a single-stream mixing layer which was approximately 30 % greater than that measured, for the same flow configuration, by Liepman & Laufer (1947). Batt (1975) subsequently showed that this particular discrepancy had probably been caused by a difference in the state of the boundary layer (laminar in the experiment of Liepman & Laufer, turbulent in that of Wygnanski & Fiedler) from which the mixing layer had developed. Tripping of the boundary layers in two-stream mixing-layer experiments, on the other hand, has been found to produce a significant reduction in the self-similar growth rate (Oster, Wygnanski & Fiedler 1977; Browand & Latigo 1979;

† Email address for correspondence: cmc7@le.ac.uk

Mungal, Hermanson & Dimotakis 1985; Bell & Mehta 1990; Karasso & Mungal 1996; Slessor, Bond & Dimotakis 1998). Because the wind tunnels used were necessarily limited in size it is not certain that all of these experimental mixing layers were truly 'fully developed' and it is possible that these differences in growth rate would have disappeared eventually had longer flow lengths been available for study. These findings do show, however, a remarkable persistence of the influence of the initial conditions, to Reynolds numbers, based on the local thickness of the mixing layer and the velocity difference across it, much higher than those commonly encountered in most practical applications.

This sensitivity of the mixing-layer growth to upstream influences is not limited to a sensitivity to the state of the boundary layers separating from the splitter plate. Numerous experiments (e.g. those of Oster & Wygnanski (1982), Fiedler & Mensing (1985) and Dziomba & Fiedler (1985)) have shown that periodic disturbances of various types introduced near the origin of the mixing layer can produce regions of nonlinear growth far downstream. These effects are observed even where the introduced perturbations are very small in amplitude in comparison with the turbulent fluctuations naturally present in the affected downstream region.

Although controversial at the time, the unexpected discovery by Brown & Roshko of ordered quasi-two-dimensional vortex-like coherent structures in what appeared to be the fully developed flow was immediately seen as very relevant to the understanding of these sensitivities for two reasons. First, it showed that mixing layers can have a turbulence structure very different from that envisaged by classical turbulence theory. Second, it suggested that Kelvin–Helmholtz instability might provide the driving mechanism for the self-similar growth of the fully developed flow. It was already well known that, in mixing layers developing from laminar boundary layers, this instability tends to cause the free shear flow to roll up on itself at a naturally preferred frequency to form a regular procession of spanwise-oriented vortices (Michalke 1965). Winant & Browand (1974) showed that natural excitation of subharmonics of the fundamental Kelvin–Helmholtz instability can cause the vortices to precess around each other and amalgamate successively in pairs and proposed this as the mechanism which drives the observed self-similar growth of the fully developed flow. Cycle-to-cycle variability in the locations of the amalgamations, it was suggested, would smooth out the step increases in the thickness of the layer and give a mean velocity profile which expanded linearly with distance from a virtual origin. In this context different initial conditions and small-amplitude perturbations introduced near the origin of the layer can be understood to affect the growth of the layer further downstream via their influence on the excitation of the Kelvin–Helmholtz modes and the preferential excitation of modes of particular frequencies (Ho & Huang 1982).

In the absence of any alternative explanation for the observed linear increase in the average scale and spacing of the structures discovered by Brown & Roshko, this idea that the self-similar growth of turbulent mixing layers is driven by sequential excitation of the subharmonics of a fundamental Kelvin–Helmholtz instability has now come to receive very widespread acceptance. Direct experimental evidence that the instability-driven vortex amalgamation process continues to be operative where mixing layers have attained full self-similarity appears to be lacking, however. At a more fundamental level doubts persist as to whether mixing layers containing organized coherent structures can ever be regarded as truly fully developed (Chandrsuda *et al.* 1978) or even whether a universal asymptotic flow state actually exists (George 1989).

The experiments of Brown & Roshko were quickly followed by others which showed that, at a certain stage in its development from a laminar initial state, the

mixing layer undergoes a definite transition from an unsteady laminar flow to one which is, in a real sense, turbulent (Konrad 1976; Breidenthal 1981). This so-called mixing transition was found to be preceded by the development, as a result of the excitation of a secondary instability, of streamise-oriented vortices on the braids or sheets of rotational fluid linking the already-existing spanwise vortices (Jimenez 1983; Lin & Corcos 1984; Lasheras, Cho & Maxworthy 1986; Bell & Mehta 1992; Rogers & Moser 1992). When these streamwise vortices have attained sufficient strength their interaction with the spanwise vortices during amalgamations of the latter generates smaller-scale turbulence and, if the local Reynolds number is high enough to sustain a continuous energy cascade, the amalgamation triggers the transition (Huang & Ho 1990).

There are thus two requirements which must be satisfied for this transition to occur: (i) a sufficient flow length for the streamwise vortices to develop; (ii) a sufficiently high Reynolds number to support the fine scales. The flow length required is typically that necessary to accommodate the initial roll-up and between two and four subsequent pairing-type amalgamations: a distance equal to a few hundred times the initial momentum thickness of the layer, θ_i. As was demonstrated by Dimotakis & Brown (1976) and Huang & Ho (1990), this is not inconsistent with the distance of $\sim 1000\theta_i$ cited by Bradshaw (1966) as the distance necessary for attainment of full self-similarity by the developing layer. Subject to (i), the transition is usually found to occur at a Reynolds number of the order of 10^4 (Dimotakis 2000). From this point on the spanwise vortices form the largest of an extended cascade of eddy scales.

The processes leading up to the mixing transition have been studied in considerable detail by experiment (Lasheras *et al.* 1986; Lasheras & Choi 1988; Huang & Ho 1990; Nygaard & Glezer 1991) and also by numerical simulation (Moser & Rogers 1991, 1993). These studies have confirmed that, despite the presence of the developing three-dimensional motions, the dynamics of the pre-transition layer usually remain dominated by the subharmonics of the fundamental Kelvin–Helmholtz instability and that the layer grows by essentially the mechanism proposed by Winant & Browand.

The situation in relation to the post-transition flow and to mixing layers that develop from turbulent boundary layers is less clear. There is abundant flow-visualization evidence that coherent structures superficially similar to the spanwise vortices present in the pre-transition flow are often present in fully turbulent mixing layers and they have been visualized clearly in compressible mixing-layer flows at local Reynolds numbers of at least 4×10^5 (Clemens & Mungal 1995). Their presence has also been educed from hot-wire measurements (Browand & Troutt 1985; Hussain & Zaman 1985) and can be inferred from some of the numerous measurements of scalar mixing that have been made in fully turbulent mixing layers by Konrad (1976), Breidenthal (1981), Mungal & Dimotakis (1984), Mungal *et al.* (1985), Koochesfahani & Dimotakis (1986), Karasso & Mungal (1996), Slessor *et al.* (1998) and Meyer, Dutton & Lucht (2006) amongst others. It has been established that the average spacing of the structures increases with their size (Brown & Roshko 1974; Dimotakis & Brown 1976; Hernan & Jimenez 1982), implying that their numbers are reduced in some way as the mixing layer grows in thickness. There is also some evidence that, in mixing layers which have developed from laminar initial conditions, the streamwise vortices survive in the post-transition flow with an average spacing which increases in step with that of the spanwise structures (Jimenez, Cogollos & Bernal 1985; Bernal & Roshko 1986; Bell & Mehta 1992). It seems that the structures are not always present however and, even in situations where their presence has been detected (Koochesfahani *et al.* 1979; Hussain & Zaman 1985), velocity correlation measurements show no

evidence of the large-amplitude antisymmetric induced fluctuations characteristic of the vortex amalgamations in the pre-transition flow (Browand & Weidman 1976).

The motivation for the present study has been provided by flow-visualization evidence showing that some spanwise-coherent structures in mixing layers undergo significant growth during the intervals between pairings or other types of large-structure interaction. This was shown first by Hernan & Jimenez (1982) who performed a very detailed statistical analysis of the coherent-structure evolution visible on one of the cine-film visualizations that had been produced earlier by the group at Caltech. Subsequent experiments carried out by Pedley (1990) (unpublished but discussed in Coats (1996)) have suggested that this continuous growth of the individual structures is to be found specifically in the post-transition part of the flow where it accounts directly for the self-similar growth of the mixing layer's thickness without any contribution at all from pairings of the pre-transition amalgamative type. Pedley also observed that, when these continuously growing coherent structures were not obviously present, there was a significant reduction in the self-similar growth rate of the mixing layer. We here present new data which corroborate and amplify Pedley's somewhat tentative findings, confirm that there is indeed a fundamental change in the growth mechanism at the mixing transition and cast fresh light on the variability of the growth rates measured with conventional traversing techniques in wind-tunnel experiments.

Flow visualization experiments remain an effective way of studying the evolution of coherent structures but flow visualization on its own has severe limitations and, especially in flows that are turbulent and thus contain three-dimensionality, caution is necessary in interpreting purely visual evidence. In a second part of this study, which is to be reported in a companion paper, several of the experiments have been replicated numerically by large-eddy simulation. These simulations have shown remarkable consistency with the experimental findings and fully support the interpretations placed here on the flow visualizations.

2. Experimental details

To visualize the convection, growth and interactions of extended sequences of spanwise-coherent structures at repetition rates of several kilohertz, the same technique of recording schlieren and shadow images on high-speed cine film as was used by Brown & Roshko (1974) and Pedley (1990) was used again in the present experiments. This required the use of dissimilar gases for the two free streams and a wind tunnel with a small test section in which high Reynolds numbers were achieved through the use of high velocities rather than large length scales. To economize as far as possible in the consumption of bottled gases, one of the two streams was of air supplied from a battery of rechargeable high-pressure tanks. In most of the experiments the second stream was of helium, argon or a mixture of the two, this providing the difference of refractive index needed to visualize the mixing layer and also allowing variation of the density ratio between the free streams. The air from the tanks could be used for either or both of the streams as required, providing long flow times for characterization of the flow in the test section by hot-wire anemometry.

The flow of each of the gases was controlled by means of a choked orifice and discharged via a perforated distributor into a settling chamber. Here it was smoothed by passage through a series of finer screens and finally accelerated into a test section of 100 mm span through a two-dimensional half-nozzle (figure 1). Where mixed helium and argon were used for one of the streams the mixing of the two gases

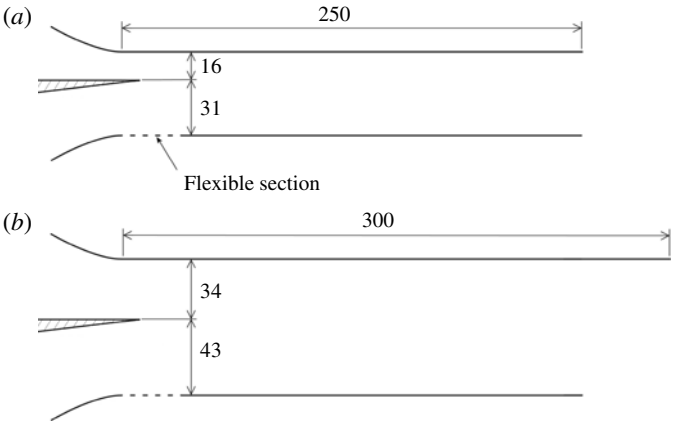

FIGURE 1. Detail of test section: (*a*) build 1; (*b*) build 2. Dimensions are in millimetres.

was carried out upstream of the settling chamber, the metering by the choked orifices allowing the mixture fraction to be set with an accuracy of better than 2 %. This was confirmed by chromatographic analysis of samples of the resulting mixture collected at the nozzle exit.

The velocity of each of the free streams was measured and recorded continuously during experiments by means of a small Pitot-static probe introduced through the wall of the test section and connected to a calibrated micromanometer. This measurement was made at a distance of 85 mm from the nozzle exit with a typical uncertainty in the dynamic head of ± 10 Pa. Velocity-profile and turbulence measurements were made with a calibrated Dantec 55P11 hot-wire probe introduced through the test-section exit and traversed automatically in the cross-stream direction with a position accuracy of ± 50 μm. A fourth-order calibration function was applied to the bridge voltage, allowing velocities to be measured with an accuracy of better than ± 2 % over the whole of the velocity range of interest. Spectral analyses of the anemometer output were performed by a fast Fourier transform (FFT) technique using a Hewlett Packard HP35670A dynamic signal analyser. The gas temperature in the settling chamber was constant to within $\pm 0.5\,^{\circ}$C throughout the extended run periods needed to map the flow within the test section.

The wind tunnel was of modular construction so that the half-nozzles and the test-section walls could be changed as necessary to suit the requirements of particular experiments. Two main configurations, designated builds 1 and 2, were used in this work, as detailed in figure 1. In both builds the velocity in the exit plane of each half-nozzle was essentially uniform (outside the wall boundary layers) in the spanwise direction, with variations of up to 3–4 % in the cross-stream direction. Most of this variation was in the region towards the outer (curved) wall of the nozzle in the part of the free stream remote from the mixing layer. The measured turbulence intensity of the flow entering the test section varied to some extent with the velocity and the area ratio of the nozzle used but was generally of the order of 0.5 %. This inlet turbulence had the character of 'white' noise with no obvious tones present in the fluctuation spectrum.

The two streams came into contact with each other 8 mm beyond the nozzle exit plane at the end of the horizontal splitter plate which separated the two settling chambers. The end of this splitter plate was tapered on the low-speed side to a knife

edge of negligible thickness which was both straight and flat to a high standard of tolerance. The momentum thicknesses of the boundary layers formed on the two sides of the splitter plate were measured as functions of the nozzle exit velocity with air as the test fluid 1 mm downstream of this trailing edge. Because the boundary layers were still laminar on separation, it was assumed that the corresponding thicknesses for the other gases could be estimated with good accuracy on the basis of Reynolds-number similarity.

The static-pressure distribution within the test section was measured by means of a differential pressure transducer with a fixed reference, connected via a scanivalve system to a total of 24 tapping points distributed along the upper and lower walls. To create free streams that were as nearly as possible uniform the angle of the hinged lower wall was adjusted once the flows were established to minimize the streamwise pressure gradients. As shown in figure 1, the hinge was formed by a flexible length of wall which ensured a smooth blend with the low-speed-side half-nozzle. With the lower wall set at its optimal angle there were small streamwise pressure gradients at the walls in the first 50 mm of the test section, associated with the adaptation of the two entry flows to the geometry of the test section and the non-self-similar initial development of the mixing layer, followed by a flow length of at least 200 mm in which the streamwise gradients were near zero. There were often small gradients at the downstream end of the test section associated with the adaptation of the flow to the unconfined conditions further downstream or, in some cases, contact between the mixing layer and either the upper or the lower wall. It is interesting to note that there was also a small but measurable pressure difference between the two streams in the part of the test section in which there was no streamwise variation of pressure. This pressure difference between the streams was also found in the numerical simulations of the same flows which are to be reported in Part 2. For experiments involving only a single moving stream the lower half-nozzle and wall were removed altogether, allowing air to be entrained directly from the laboratory. Ducting was rigged to shield the inflow of entrained air from draughts but no attempt was made to smooth the entrained flow itself.

To facilitate flow visualization the sidewalls of the test section were formed by sheets of 8 mm thick aberration-free float glass. The visualization was effected by means of a folded schlieren system with an offset angle of 5°, based on a pair of 305 mm diameter front-silvered concave mirrors of focal length 2.44 m. The light emitted by the source lamp was focused on a 1 mm diameter pinhole placed at the focus of the first mirror and a matching pinhole was positioned at the focus of the second mirror as the schlieren stop. The features of the flow shown most clearly by this optical arrangement were the braids connecting the spanwise-oriented large structures. For the production of shadowgraphs showing the fine-scale turbulence the second pinhole was removed. With both arrangements neutral-density filters were used to optimize the system sensitivity. In a number of the experiments simultaneous side- and plan-view visualizations were produced by the introduction of a second pair of plane front-silvered mirrors positioned above and below the test section. For these experiments the instrumented upper and lower test-section walls were replaced with otherwise identical components incorporating large areas of transparency in place of the pressure tappings.

High-definition images of the fine-scale turbulence were recorded with a 35 mm SLR camera fitted with a zoom lens, using a microsecond argon-jet spark as the light source. For tracking the convection, growth and interaction of the large structures in real time a 75 W xenon arc lamp was used as the light source and the images

were recorded on 100-foot lengths of 16 mm cine film by a high-speed rotating-prism camera operated at a rate of 4000 fps. The exposure time of the individual frames with the camera operating at this speed was 100 μs. An accurate time base was marked on the film to allow correction for variations in the camera speed. For detailed analysis the recorded images were copied onto videotape and then digitized frame by frame.

More than 50 cine films of varying quality were produced in total, approximately half of which were analysed in some detail. The largest number of these were of mixing layers of uniform density formed between a high-speed stream composed of a mixture of 70 % argon and 30 % helium and a low-speed stream of air. The velocities of the two streams, denoted U_1 and U_2 respectively, were varied separately within the ranges 9–32 and 2–13 m s^{-1} to cover a range of velocity ratios at different Reynolds numbers. The velocity ratios were chosen to give values of the parameter

$$R = \frac{U_1 - U_2}{U_1 + U_2} \tag{2.1}$$

in the range 0.41–0.63. As is well known, the spatial growth rates of uniform-density mixing layers vary approximately in proportion to R. The resulting value of the Reynolds number

$$Re = \frac{(U_1 - U_2)\,\delta_{vis}}{\nu} \tag{2.2}$$

at a reference distance of 250 mm from the splitter plate ranged from $\sim 2 \times 10^4$ to $\sim 8 \times 10^4$, depending on the particular velocities and velocity ratio chosen.

The length scale used here, δ_{vis}, is the same visual thickness obtained by drawing straight-line mean tangents to the edges of the visualized mixing layer as was used by Brown & Roshko (1974). This is not a precise method of measurement but, as those authors showed, the thickness measured in this way corresponds closely in practice to that defined by the edges of the mixing layer as determined from mean scalar and velocity profiles. It also provides a convenient means of relating directly the mean growth of the layer as a whole to the growth of the individual structures within it. Most of the tests involving growth to only small values of δ_{vis} were performed with test-section build 1 and those involving the higher rates of growth with build 2. Some tests were replicated with both builds, however, to check that the development of the mixing layer had not been influenced in any way by wall proximity effects.

The kinematic viscosity ν used here in the calculation of Re is that of the homogeneous fluid formed within the mixing layer by mixing together the fluids drawn from the two streams in the proportions predicted by the entrainment-ratio formula of Dimotakis (1986). All mixture viscosities in this work have been calculated from the semiempirical formula of Wilke (1950). For a number of the above uniform-density test conditions, profiles of mean and fluctuating velocity were measured to complement the flow visualizations in runs of longer duration in which air was substituted for the argon–helium mixture in the faster stream. The kinematic viscosity of the argon–helium mix was slightly greater than that of the air (sufficient to produce a difference of ~12 % in the momentum thickness of the separating boundary layer) and so the main effect on the flow of this change of gas is expected to have been a correspondingly small displacement in the average location of the mixing transition.

To study the effects of density differences between the free streams a number of visualization runs were also conducted in which: (i) pure helium was used for the high-speed stream and air for the low-speed stream, giving a free-stream density ratio ρ_2/ρ_1 of 7.2; (ii) these two gases were interchanged, giving a density ratio of 0.14. Finally,

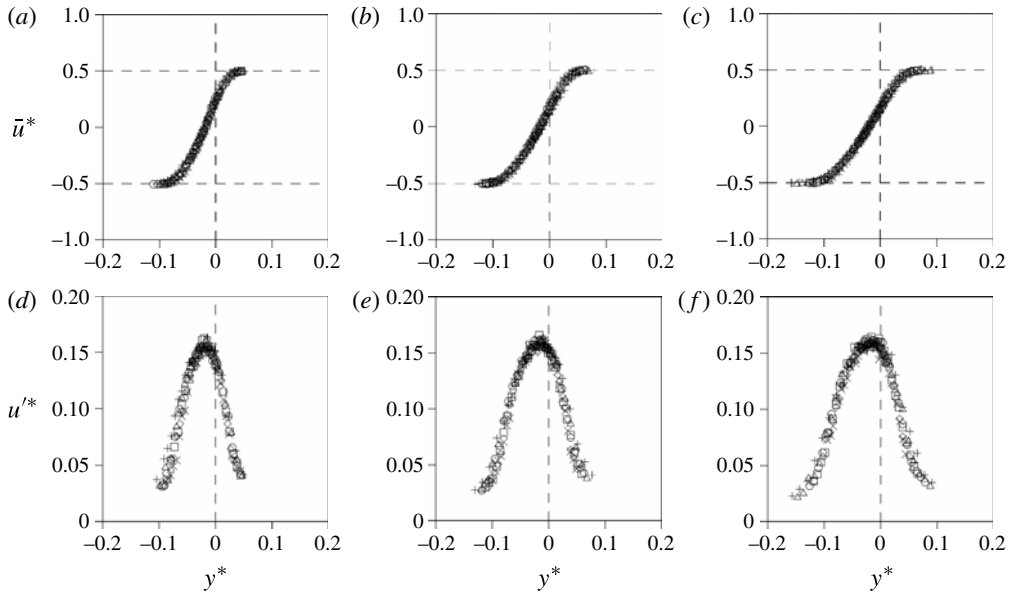

FIGURE 2. Non-dimensionalized profiles of (*a–c*) mean velocity and (*d–f*) r.m.s. of velocity fluctuations: (*a*,*d*) $U_1 = 32.0$ m s^{-1}, $U_2 = 12.9$ m s^{-1}; (*b*,*e*) $U_1 = 32.1$ m s^{-1}, $U_2 = 9.6$ m s^{-1}; (*c*,*f*) $U_1 = 31.9$ m s^{-1}, $U_2 = 7.2$ m s^{-1}; $\rho_2/\rho_1 = 1.0$. Measurements made at distances of 72 mm (crosses), 97 mm (triangles), 122 mm (circles), 147 mm (squares), 172 mm (diamonds) and 197 mm (diagonal crosses) from the splitter plate.

to access higher spatial growth rates and Reynolds numbers, the low-speed half-nozzle and lower wall of the test section were removed, creating a half-jet configuration ($R = 1$) in which a single moving stream was allowed to entrain quiescent air from the laboratory. Visualization runs were conducted with (i) the 70 % argon/ 30 % helium mix ($\rho_2/\rho_1 = 1.0$), (ii) a 30 % argon/ 70 % helium mix ($\rho_2/\rho_1 = 2.0$) and (iii) pure helium ($\rho_2/\rho_1 = 7.2$) as the moving stream. Runs with pure argon as the moving stream were also attempted but did not produce visualizations of usable quality. Free-stream velocities of up to 60 m s^{-1} were used in these variable-density and single-stream tests and, in one uniform-density single-stream case, a Reynolds number approaching 2×10^5 was attained at a distance of 250 mm from the splitter plate.

3. Results

3.1. *Similarity characteristics*

That the developed experimental flows were self-similar and had the characteristics expected of fully turbulent mixing layers is shown by the representative mean- and fluctuating-velocity profiles for conditions of uniform density and three different values of R presented in figure 2. The local mean velocity $\bar{u}(x, y)$ and the root-mean-square (r.m.s.) of the local velocity fluctuation $u'(x, y, t)$ are plotted as the non-dimensional variables

$$\bar{u}^* = \frac{\bar{u} - U_C}{U_1 - U_2}, \quad u\prime^* = \frac{\sqrt{\overline{u'^2}}}{U_1 - U_2} \tag{3.1}$$

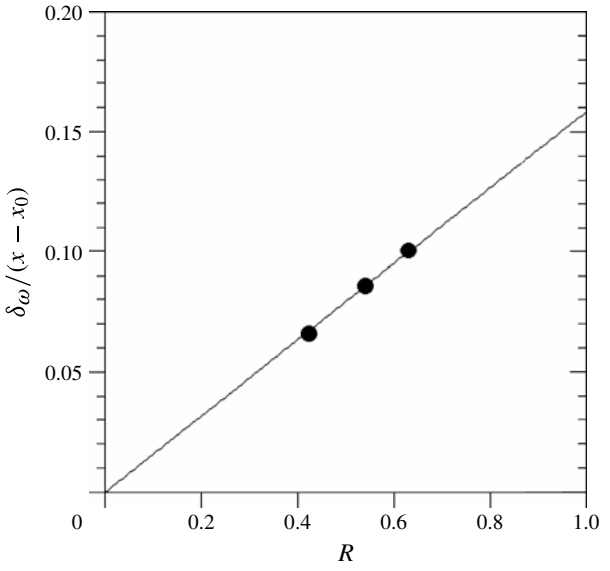

FIGURE 3. Vorticity-thickness growth rate versus non-dimensionalized velocity difference between free streams; datum points computed from data presented in figure 2(*a–c*).

where

$$U_C = \frac{U_1 + U_2}{2}. \tag{3.2}$$

The abscissa is the non-dimensionalized cross-stream coordinate

$$y^* = \frac{y - y_0}{x - x_0} \tag{3.3}$$

where x and y are, respectively, the streamwise and cross-stream coordinates of position and (x_0, y_0) is the virtual origin of the mixing layer. As expected at these free-stream velocities, the profiles of both variables approach self-similarity fairly rapidly beyond the first traverse plane and the peak turbulence intensities are in the expected range. Similar profiles were obtained at lower free-stream velocities but with longer flow lengths required to attain full self-similarity.

The rate of growth with x of the vorticity thickness of the mixing layer,

$$\delta_\omega = \frac{U_1 - U_2}{(\partial \bar{u}/\partial y)_{max}}, \tag{3.4}$$

has been determined from the mean velocity profiles in figure 2 and is plotted as a function of R in figure 3 where the three datum points are seen to be well fitted by a straight line of gradient 0.16 passing through the origin of the coordinates. This gradient also is within the range of scatter of previously published measurements (Brown & Roshko 1974).

3.2. *The mixing transition*

That the experimental mixing layers underwent the mixing transition described and discussed in § 1 was shown by the evolution of the velocity-fluctuation spectrum at the centre of the layer. Jimenez (1983) and Huang & Ho (1990) have both demonstrated

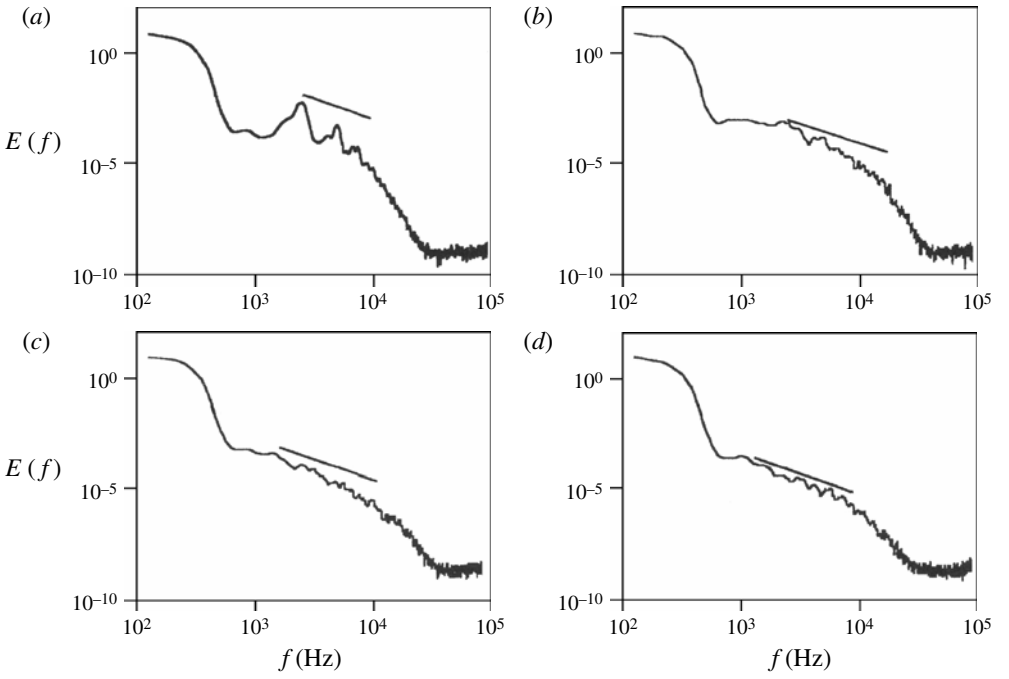

FIGURE 4. Power spectrum of velocity fluctuations at centre of mixing layer at distances of (*a*) 5 mm, (*b*) 15 mm, (*c*) 75 mm and (*d*) 110 mm from the splitter plate; $U_1 = 20.7$ m s^{-1}, $U_2 = 5.4$ m s^{-1}, $\rho_2/\rho_1 = 1.0$. The reference line indicates roll-off rate of fully developed inertial cascade.

that the transition is accompanied by the establishment of a cascade of eddy scales in which the spectrum level $E(f)$ of the fluctuation energy varies with frequency f as $E \propto f^n$ and the roll-off exponent n attains the limiting value $-5/3$. This is the value implied for the inertial subrange of isotropic turbulence by Kolmogorov's (1941) universal equilibrium theory. Figure 4 shows some representative spectra sampled at different values of x and plotted on logarithmic axes for one particular set of experimental conditions. Also shown extending over the relevant range of frequencies for each spectrum is a reference line of gradient $-5/3$, indicating the roll-off rate of the fully developed inertial cascade. As in the experiments of Jimenez and Huang & Ho, the relevant part of the spectrum was initially dominated by a few large peaks, corresponding to the fundamental Kelvin–Helmholtz instability and its subharmonics (figure 4*a*). Further downstream a cascade of smaller scales appeared but with a steeper roll-off than in fully turbulent flow, indicating that the smaller scales were still far from isotropic (figure 4(*b*,*c*)). Further downstream again the roll-off rate relaxed to that characteristic of fully turbulent flow (figure 4*d*) and remained unchanged thereafter.

Hot-wire measurements of the type presented in figure 4 could not be made in flows involving the mixing of different gases and so it was necessary also to be able to identify the location of the mixing transition directly from the flow visualizations. Real-time visualizations in fact provide more useful information than spectral measurements because, as was discussed in § 1, although the lead-up to the transition is a gradual process, the transition itself is associated with a highly

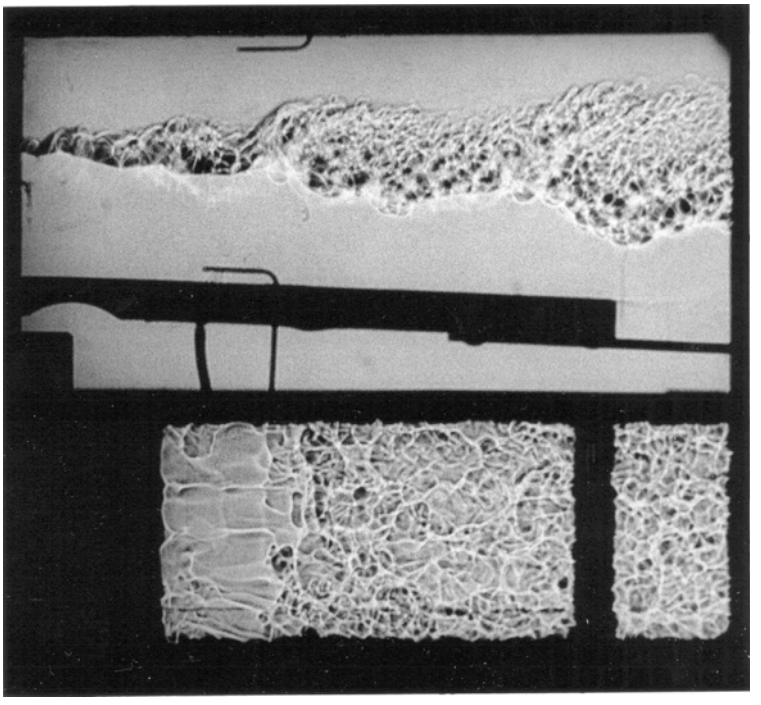

FIGURE 5. Simultaneous side- and plan-view spark shadowgraph showing mixing transition; $U_1 = 13.1$ m s^{-1} (helium), $U_2 = 3.0$ m s^{-1} (air).

localized vortex amalgamation 'event'. In mixing layers which develop naturally from a laminar initial state against a background of low-level fluctuations covering a broad band of frequencies there is a large degree of randomness in the locations of the initial roll-up and the subsequent vortex amalgamations. Spectral measurements are long-time averages and so do not locate the triggering amalgamation on the required time-resolved basis.

Figure 5 shows a simultaneous side- and plan-view visualization in which the optical set-up has been adjusted to highlight the small-scale turbulence in the flow. It will be noted in the side view that the angle at which the lower wall of the test section has been set to eliminate the streamwise pressure gradient at these particular flow conditions produces a diverging channel. This is because the displacement thickness of a mixing layer is a function of the free-stream density ratio as well as R and has a growth rate which becomes positive at intermediate values of R for $\rho_2 \gg \rho_1$. The same can be seen in the corresponding side-view visualizations reproduced in Brown & Roshko (1974).

The plan view in figure 5 shows very clearly how the unsteady laminar flow in the initial part of the layer, in which the secondary streamwise vortices are the most prominent features, is abruptly replaced at a particular streamwise location by a flow which is suffused with small three-dimensional eddies. Reference to the side view shows that this is the location at which two spanwise vortices are in the process of amalgamation. Tracking of the instantaneous transition location as a function of time produces an irregular sawtooth-type waveform, the transition point in the flow convecting downstream with the amalgamating vortices and then jumping upstream

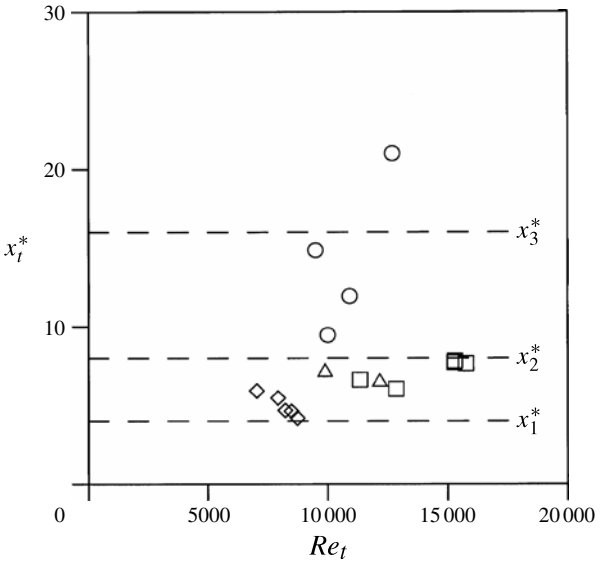

FIGURE 6. Mean transition location versus transition Reynolds number: $\rho_2/\rho_1 = 1.0$ (circles and squares), 7.2 (diamonds) and 0.14 (triangles). Circles indicate measurements made with nozzle/test-section build 1; all other measurements made with nozzle/test-section build 2.

as the amalgamation of the following pair of vortices becomes the next transition event. The individual amalgamations could be observed clearly in the side-view cine sequences and there were recognizable differences in the appearance of the spanwise-coherent structures and their linking braids pre- and post-transition as visualized in side view by either shadow or schlieren. There was therefore no difficulty in practice in tracking the instantaneous transition location from the cine side views alone.

To demonstrate that the transition location x_t determined in this way was consistent with the two transition criteria discussed in § 1, the average values of x_t determined from analyses of 16 of the cine films are plotted against the Reynolds number of the mixing layer at the average transition location in figure 6. The data shown embrace different free-stream velocities and velocity ratios, different density ratios and both builds of the test section. To relate these average x_t values, at least notionally, to the expected locations of the successive vortex amalgamations they have been plotted here in normalized form as a variant of the 'pairing parameter' first proposed by Huang & Ho (1990). This parameter is based on the assumption that the initial roll-up is followed by a sequence of pairing amalgamations produced by excitation of the subharmonics of the fundamental Kelvin–Helmholtz mode and that the fundamental instability wave and its subharmonics all convect downstream at the same velocity. The distances from the separation point to the locations of the successive amalgamations, x_i ($i = 1, 2, 3, \ldots$), must then be expected to scale on the wavelength of the fundamental mode, L_0, and to vary in inverse proportion to the averaged spatial growth rate. For mixing layers of uniform density this leads to the parameter

$$x_i^* = \frac{Rx_i}{L_0} \tag{3.5}$$

as an appropriate normalization for x_i. In their own experiments on mixing layers developing naturally from laminar initial conditions Huang & Ho found that the first

three amalgamations occurred at values of x_i^* close to 4, 8 and 16 and that the transition was usually triggered by the second of them.

To apply the same reference values of x_i^* to mixing layers formed between streams of different densities it is necessary to consider the effects of the density ratio on both L_0 and the spatial growth rate. In evaluating their uniform-density pairing parameter Huang & Ho assumed that

$$L_0 = U_C/f_0 \tag{3.6}$$

with the frequency of the initial roll-up, f_0, given by

$$\frac{f_0\theta_1}{U_C} \approx 0.034 \tag{3.7}$$

where θ_1 is the momentum thickness of the boundary layer formed on the high-speed side of the splitter plate. Their choice of θ_1, as the normalizing length scale in (3.7) was based on their earlier experimental finding (Ho & Huang 1982) that, in a two-stream mixing layer, it was the inflection formed transiently on the high-speed side during the merging of the two boundary layers that was most receptive to high-frequency disturbances and determined the frequency of the fundamental Kelvin–Helmholtz mode. The value 0.034 in (3.7) was that given by linear stability theory for a mixing layer with a tanh profile of momentum thickness equal to θ_1 (Monkewitz & Huerre 1982) and applied, to a good approximation, for all values of R. Now analysis of the temporal instability of variable-density mixing layers (Michalke 1971) suggests that, if it continues to be the inflection formed transiently in the separated high-speed-side boundary layer that remains dominant, f_0 will not be greatly affected by the density of the fluid on the low-speed side of the splitter plate. It then follows that, because the wave velocity (represented by U_C) is self-cancelling in the calculation, combination of (3.6) and (3.7) gives the same fundamental wavelength $L_0 \approx \theta_1/0.034$ for all density ratios as well as for all values of R.

By the same argument, Michalke's analysis suggests that the effect of the density variation on the temporal growth rates of the excited modes is also likely to be fairly small, at least during their early linear stages. If this is in fact the case, the effect of the density difference between the free streams on the spatial growth rate can be estimated to a first approximation by applying a simple Galilean transformation to the same temporal growth rate. The more general form of (3.2) which must be used in the case of a mixing layer formed between streams of different densities is

$$U_C = \frac{U_1 + U_2}{2}\left(1 + \frac{\sqrt{\rho_1} - \sqrt{\rho_2}}{\sqrt{\rho_1} + \sqrt{\rho_2}}R\right) \tag{3.8}$$

(Coles 1981) and so the pairing parameter becomes

$$x_i^* = \frac{0.017\,(U_1 - U_2)\,x_i}{U_C\theta_1}. \tag{3.9}$$

This reduces to (3.5) in the uniform-density case and places the amalgamations at approximately the same values of x_i^* for all density ratios.

The average values of x_t plotted with this normalization in figure 6 show the transition as having occurred in the expected range of Reynolds numbers and been triggered typically by the second or third amalgamation. It should be noted, however, that the vortices did not always amalgamate sequentially in pairs. The cine films showed that, not infrequently, three or even four small vortices would

amalgamate simultaneously under the influence of a lower subharmonic of the initial roll-up frequency or a smaller-than-average vortex would become caught up in an amalgamation of two larger vortices. The trend to larger x_t^* values in build 1 of the wind tunnel presumably reflects the influence of the larger nozzle contraction ratio on the low-level background turbulence. The apparent trend to smaller x_t^* values in the runs for which $\rho_2 > \rho_1$, on the other hand, reflects the approximate nature of the assumptions made in the derivation of (3.9). The cine-film evidence indicated that the actual f_0 values for these runs were somewhat higher than predicted by (3.7), possibly because the greater inertia of the fluid on the low-speed side of the splitter plate had affected to some extent the evolution of the inflected velocity profile during the merging of the two boundary layers.

The data presented in figure 6 give a high level of confidence that the vortex amalgamations which triggered the transition had been identified correctly from the side-view visualizations. With the instantaneous transition location clearly identified in this way it was then possible to examine the pre- and post-transition parts of the mixing layer separately on a time-resolved basis.

3.3. *Large-structure growth and interaction*

The first main objective of this study was to characterize the growth and interactions undergone by the organized large structures visible in the fully turbulent part of the mixing layer downstream of the mixing transition for comparison with the vortex evolution in the pre-transition flow. For this purpose the spanwise-integrated picture of the flow provided by the visualization techniques used here was more useful than a planar view because: (i) the presence of a visible large-scale structure in the side views was itself positive evidence of a high degree of local spanwise coherence in the flow; (ii) the visualizations showed directly the relationship between the large-structure evolution and the spanwise-averaged growth of the mixing layer as a whole.

The techniques employed to track the evolution of the individual structures were the same as those used by Pedley (1990). Extended sequences of digitized images, enhanced where necessary by a limited amount of filtering and contrast adjustment, were examined systematically and all of the coherent structures which were clearly visible in each image were identified individually. In the shadowgraphs of the post-transition flow these showed themselves as more or less regular symmetrical bulges in the band of turbulent fluid which formed the bulk of the mixing layer, often with tongues of entrained irrotational fluid clearly visible in the spaces between (figure 7*a*). That these symmetrical bulges did in fact mark the presence of vortex-like coherent structures was very evident when the images were viewed in rapid sequence, the convection of each bulge being accompanied by the visible rotation of the smaller eddies contained within it around a common centre in what appeared to approximate to a solid-body motion. In the schlieren images it was the inclined interfacial braids linking the large structures that stood out most clearly (figure 7*b*). In the post-transition flow these were diffuse in appearance and showed clear evidence of being suffused with smaller-scale turbulence.

Once the structures had been identified, the coordinates of the two polar points of the circle which best fitted the visible traces of the outline of each structure (figure 8*a*) were logged and tracked from frame to frame. The centre of this circle was taken as the centre of the rotation. Some subjectivity was involved in the fitting procedure but, because it was carried out in a consistent way throughout the analysis of each image sequence, the reliability of the general findings is not in any doubt. The patterns

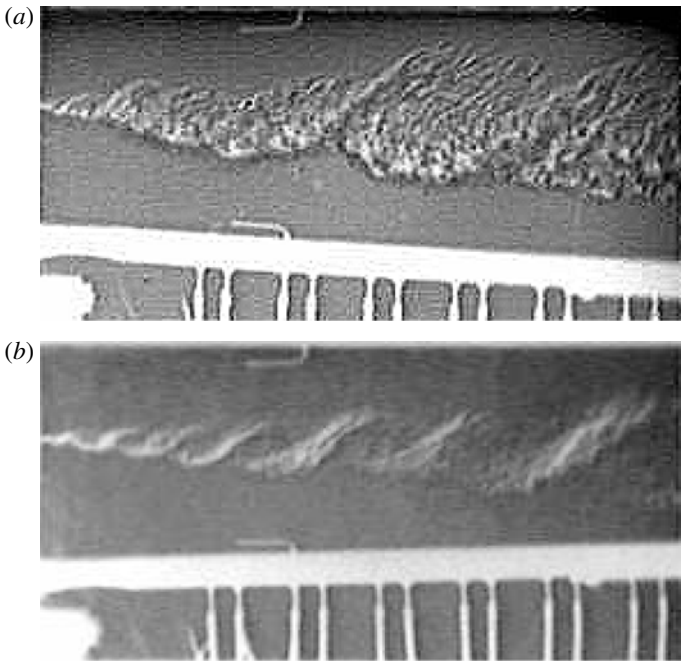

FIGURE 7. Representative instantaneous side views of predominantly post-transition mixing layers: (*a*) shadowgraph for $U_1 = 32.6$ m s^{-1}, $U_2 = 7.8$ m s^{-1}, $\rho_2/\rho_1 = 7.2$; (*b*) schlieren image for $U_1 = 20.2$ m s^{-1}, $U_2 = 7.1$ m s^{-1}, $\rho_2/\rho_1 = 1.0$.

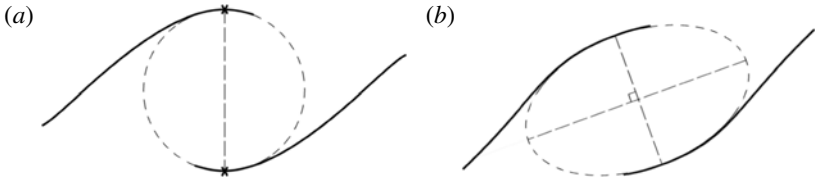

FIGURE 8. (*a*) Polar points used to track convection and growth of individual large structures. (*b*) Elliptical mapping of large structures employed by Hernan & Jimenez (1982).

of evolution shown by the detailed tracking could be readily confirmed by direct slow-motion viewing of the original cine films.

As a reference against which the evolution of the post-transition structures can be compared figure 9 presents some representative time traces illustrating the familiar pattern of growth by amalgamation in the pre-transition mixing layer. The particular traces shown were produced from the analysis of two short image sequences chosen more or less at random for different flow conditions. In both cases the image sequences used had been produced by the schlieren technique which, in the pre-transition flow, visualized the interface between the two fluids very sharply. The two polar points logged in the tracking (figure 8*a*) lay unambiguously on the outermost turn of the spiralling interface with extended the linking braids into the individual vortices.

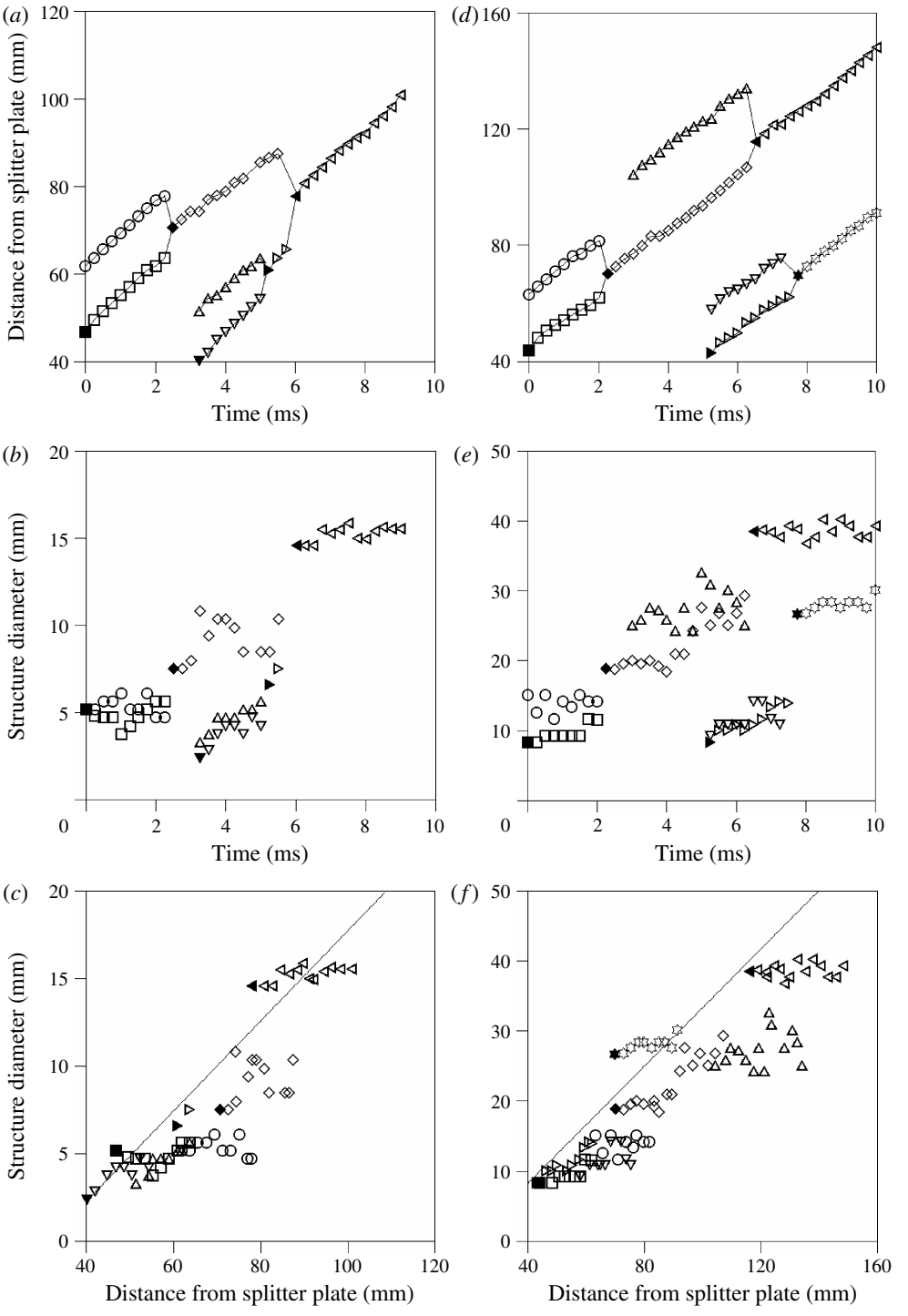

FIGURE 9. Pre-transition vortex evolution: (*a–c*) $U_1 = 9.6$ m s^{-1}, $U_2 = 2.2$ m s^{-1}, $\rho_2/\rho_1 = 1.0$; (*d–f*) $U_1 = 18.1$ m s^{-1}, $U_2 = 4.3$ m s^{-1}, $\rho_2/\rho_1 = 7.2$. Within each set of plots the same symbols are used to identify the individual vortices. The reference lines in (*c*,*f*) are least-squares fits to the filled symbols only.

Figure 9(*a*) shows that the vortices all convected downstream at velocities close to that given by (3.8) and that, at particular times, a pair of vortex tracks was replaced by a single new track as the two vortices amalgamated. Figure 9(*b*) shows, for the same sequence, how the diameters of the individual vortices (defined as in figure 8*a*) remained almost constant throughout most of their lifetimes but increased in a stepwise manner with each amalgamation. In figure 9(*c*) the same data are replotted to show the relationship between the spatial growth of the individual vortices and that of the mixing layer as a whole. The reference line in this plot is a least-squares fit to just the datum points corresponding to the conditions immediately following the amalgamations (identified by the filled symbols) and can be taken to represent the average spatial growth rate of the pre-transition part of the mixing layer. (Note that the fit is not a particularly close one because the mixing layer attains full self-similarity only downstream of the mixing transition and because the randomness with which the fundamental Kelvin–Helmholtz mode and its subharmonics are excited has the effect of introducing jitter into the location of the virtual origin.) It can be seen very clearly from this third plot that the growth of the layer as a whole was also associated with the amalgamations. As the participating vortices began to interact they underwent progressive displacement in the cross-stream direction and precessed around each other in pairs with a consequent large entrainment of irrotational fluid from the free streams. These cross-stream displacements, corresponding to the growing subharmonics of the fundamental Kelvin–Helmholtz instability, increased in magnitude until the two vortices had precessed through an angle of 90° at which point they amalgamated to form a single new vortex. Figure 9(*d–f*) shows exactly the same pattern of evolution in a pre-transition mixing layer of non-uniform density.

Figure 10 presents the corresponding time traces produced from two representative image sequences illustrating the pattern of evolution in the post-transition mixing layer. Here the spanwise-coherent large structures revealed by the visualization were not two-dimensional spiral vortices but turbulent vortex cores and the polar points logged in the tracking (figure 8*a*) marked the extremities of these turbulent cores. Figure 10(*a*)–(*c*) were produced from the analysis of schlieren images and figure 10(*d*)–(*f*) from the analysis of shadowgraphs but the two visualization techniques led to essentially identical results. Once again the first image sequence was of a uniform-density mixing layer and the second of a mixing layer formed between streams of different densities.

Figure 10(*a*,*d*) show that, as in the pre-transition mixing layer, the large structures all convected downstream at a near-constant velocity and that, at particular times, pairs of tracks were replaced by single new tracks as neighbouring structures interacted with each other. When Brown & Roshko (1974) produced similar tracks from their own cine-film visualizations of high-Reynolds-number mixing layers 40 years ago they took them as evidence that the fully turbulent mixing layer grows by the same instability-driven mechanism as seen in figure 9, an interpretation that has received widespread uncritical acceptance ever since. However, simultaneous direct tracking of the growth of the individual large structures shows this interpretation to be incorrect. It is seen in figure 10(*b*,*e*) that, in contrast with the situation in the pre-transition layer, the diameters of the individual structures all grew continuously at a constant rate between interactions. It is seen further in figure 10(*c*,*f*) that this continuous linear growth of the individual structures matched and defined the self-similar growth of the mixing layer as a whole. The growth of the layer thus occurred as a continuous inflow from the free streams to feed the growth of the rotating turbulent structures within it without those structures undergoing any displacements at all in the cross-stream direction.

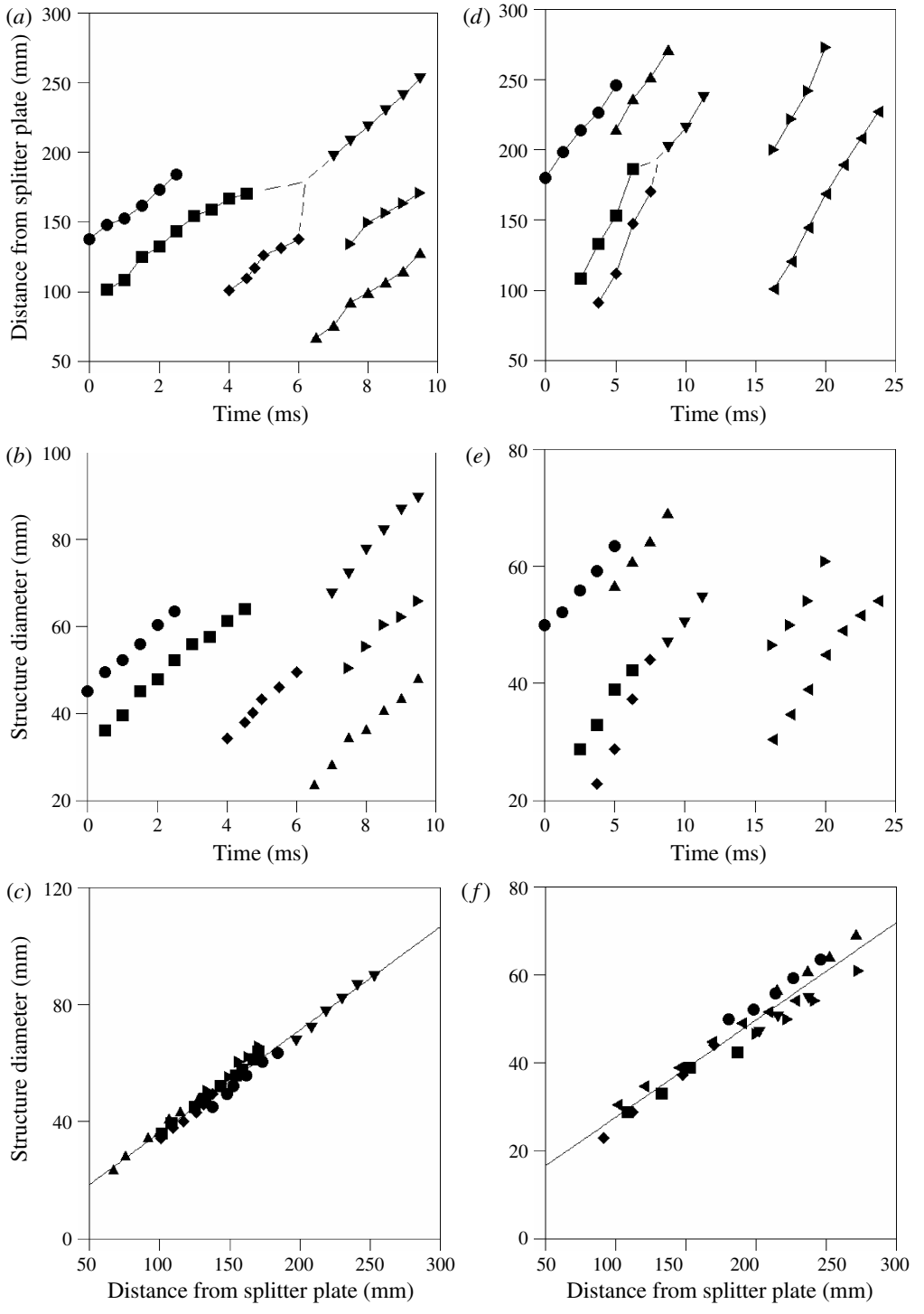

FIGURE 10. Post-transition large-structure evolution: (*a–c*) $U_1 = 20.9\ \mathrm{m\ s^{-1}}$, $U_2 = 0$, $\rho_2/\rho_1 = 1.0$; (*d–f*) $U_1 = 32.6\ \mathrm{m\ s^{-1}}$, $U_2 = 7.8\ \mathrm{m\ s^{-1}}$, $\rho_2/\rho_1 = 7.2$. Within each set of plots the same symbols are used to identify the individual structures.

What is remarkable about the data in this figure is not that the turbulent cores of these vortex-like structures grow continuously but that the growth continues at the same constant rate in all of them throughout their lifetimes. If each structure had been formed as a result of the excitation of a subharmonic of the fundamental Kelvin–Helmholtz instability one might expect the subsequent outward turbulent diffusion of the concentrated vorticity to cause a continuous increase in the size of the core. On dimensional grounds, however, its diameter should then increase as the square root of time, not linearly (Moore & Saffman 1975). Alternatively, if each growing structure was a fresh roll-up in progress, driven by the excitation of the Kelvin–Helmholtz instability of the local mean velocity profile, one would expect to see its growth rate first increase to a maximum and then fall away again as the surrounding fluid became denuded of vorticity and the instability saturated. The continuous linear growth seen in this figure indicates that something more complicated than two-dimensional diffusion and induction is occurring here.

Detailed study of the cine films confirmed that the large-structure interactions which occurred in the post-transition mixing layer were all quite different in character from those which occurred in the pre-transition flow. The most common type, represented by the merging tracks marked with the broken lines in figure 10(*a*,*d*), occurred when two neighbouring structures had grown to the point at which their rotations were interfering with each other. Both structures then appeared to break down and, in most cases, were replaced a short time later by a single new structure which resumed the continuous linear growth of its parents. In contrast with their pre-transition counterparts, these post-transition pairing interactions involved no visible displacement of the participating structures in the cross-stream direction and contributed nothing to the growth of either the individual structures or the mixing layer as a whole. The diameters of the visible structures plotted in figure 10(*b*,*e*) indicate that the new rotational structures which emerged from the pairing interactions tracked in figure 10(*a*,*d*) (identified in the figure by the inverted triangles) contained little more than half the fluid that had been contained within their parents. The remainder of this fluid had been returned to the regions of induced flow between the continuously growing rotational structures. These interactions were thus very clearly a consequence of the growth of the individual structures, not its cause.

Not all of the interactions in the post-transition mixing layer were of this pairing type, however. Not infrequently a structure which found itself closely confined by both of its immediate neighbours would cease growing, become elliptical in shape and then flatten to form a new inclined braid directly linking the two structures that remained. This sacrificial type of interaction was the same as that described by Damms & Küchemann (1974) and reported by Hernan & Jimenez (1982) and could be identified in the tracking as the simple termination of a single track between two others which continued unaffected. The 'tearing' type of interaction seen also by Hernan & Jimenez and by Pedley (1990) can be regarded as a variant of this sacrificial type. The common feature shared by all of the interactions in the post-transition layer was that they functioned to relieve at intervals the crowding resulting from the continuous growth of the individual structures, thus allowing the growth of those that remained to continue unimpeded. In this way a constant average large-structure spacing:diameter ratio was maintained in the post-transition flow as the mixing layer increased in thickness.

The patterns seen in figure 10 and described above were entirely typical of the post-transition flow and could have been illustrated by any number of sequences taken from any of twenty or more cine films covering different free-stream density ratios and different values of R. It should also be noted that the change in the

pattern of large-structure growth and interaction from that of figure 9 to that of figure 10 always coincided with the mixing transition and was definitely not an effect of wall proximity. This was verified experimentally by performing duplicate runs for selected free-stream conditions in both the larger and smaller builds of the test section. That the walls of the test section were far enough away from the mixing layer not to have interfered with the excitation of the subharmonics of the fundamental Kelvin–Helmholtz instability was also indicated by theory. Moore & Saffman (1975) have shown mathematically that the induced cross-stream displacements associated with vortex amalgamations of the pre-transition type are not affected significantly by wall reflection effects until the distance between the centreline of the mixing layer and the reflecting wall becomes much less than the distance separating the vortex centres. In most of the experiments performed here the mean transition location lay well within the first half of the available length of free flow and this criterion was satisfied very comfortably.

In some of the experiments the growth of the mixing layer and/or the angle of the lower wall of the test section were such that the layer made direct contact with one of the walls far downstream of the mixing transition and long after the growth pattern of figure 9 had been replaced by that of figure 10. Hot-wire measurements showed that, where this occurred, the increasing proximity of the wall caused some modification of the velocity fluctuations induced in the free stream, as in the experiments of Wood & Bradshaw (1982). However, the flow visualizations showed that this had little effect on the flow internal to the mixing layer, the continuous linear growth of the large structures continuing almost to the point of impingement.

It should be noted that the post-transition pairing-type interactions described above did not always give rise to a new structure to fill the gap in the procession left by its two predecessors. The breakdown of the interacting pair of structures was sometimes followed instead by a more general breakdown of the visible large-scale organization in the post-transition flow. This persisted until a stronger-than-average vortex was generated in the pre-transition part of the layer and, somewhat in the manner of the leading vortex in an impulsively started flow, established a new procession of post-transition structures in its wake. The periods of organized flow downstream of the transition location thus alternated with periods of variable length during which no coherent structures were visible in the turbulent part of the layer.

The proportion of the total flow time during which the turbulence was in its organized state was measured systematically for various free-stream conditions and is presented in figure 11 as a function of the density ratio and two different measures of the extent to which the mixing layer might be considered to have become fully developed within the available flow length. These were the local Reynolds number of the mixing layer and the pairing parameter x_i^*, both evaluated at a distance of 250 mm from the splitter plate. The important difference between these two measures is that x_i^* incorporates an influence of the initial conditions whilst the Reynolds number does not.

The results presented in figure 11 were all obtained in the build 2 test section. They show a heavy predominance of organized over disorganized flow in uniform-density mixing layers but with more and/or longer periods of disorganized flow when the free streams were of different densities. More detailed consideration of just the experiments in which R was held constant (the datum points distinguished by the filled symbols) suggests that, in the case of non-uniform density, the periods of disorganized flow also increased with the spatial growth rate of the mixing layer (which itself increased with

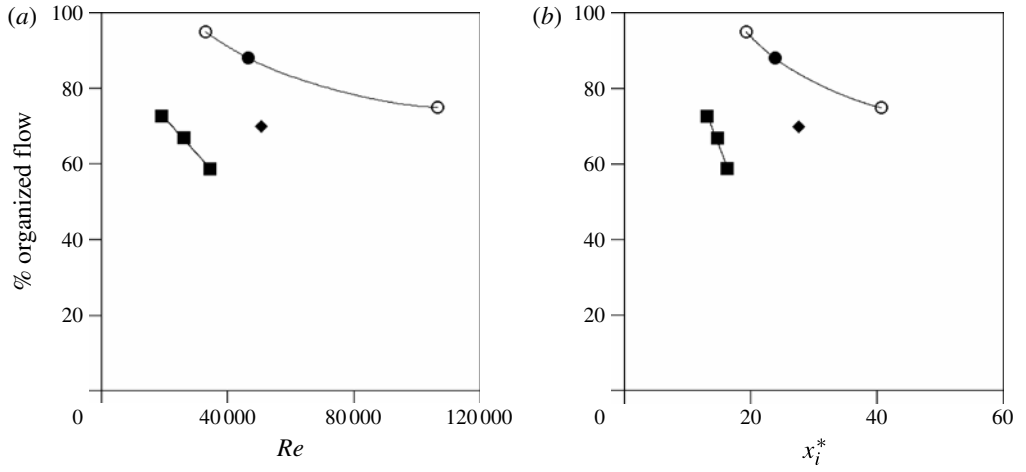

FIGURE 11. Extent of large-scale organization in the post-transition mixing layer (build 2 test section) versus (*a*) Reynolds number and (*b*) pairing parameter at a distance of 250 mm from the splitter plate: $\rho_2/\rho_1 = 1.0$ (circles), 7.2 (squares) and 0.14 (diamond). Filled symbols indicate test conditions for which $R \sim 0.6$.

ρ_2/ρ_1). With both uniform and non-uniform densities the periods of disorganization tended to increase as the flow became more fully developed.

The cine-film visualizations obtained with the build 1 test section showed the same trend to reduced levels of organization with increasing flow development but, at comparable Reynolds numbers, these levels were noticeably lower than in the build 2 test section. The x_i^* values in the build 1 test section were roughly twice as great as those presented in figure 11(*b*), however, suggesting that it is the pairing parameter that provides the more relevant measure of the flow development. This could imply that the initial conditions have a continuing influence on the post-transition mixing layer (discussed in § 1) through their effect on the rate of decay of the flow organization with increasing streamwise distance.

Similar breakdowns of the organized flow downstream of the transition location were observed by Pedley (1990) who also reported that the periods of disorganized flow tended to increase with the spatial growth rate of the layer. It is not clear from his data to what extent this apparent trend was separate from any dependence on the Reynolds number or x_i^*. It may be noted that intermittent disappearance of the large-scale organization was also observed in the aqueous mixing-layer experiments of Karasso & Mungal (1996) and that these authors also found that the periods of disorganized flow tended to increase with the Reynolds number.

3.4. *Influence of large-scale organization on mixing-layer growth and entrainment*

The second main focus of interest in this study was the effect of the presence or absence of the large-scale organization on the similarity characteristics of the post-transition mixing layer. The filled symbols in figure 12 show, for a range of different density ratios and values of R, the measured average rate of growth of the visual thickness of the post-transition layer during the periods in which the processions of coherent structures were clearly visible. The least-squares fits to these measurements show the same trends as those in the comparable plot presented by Brown & Roshko (1974), i.e. increasing growth rate with both ρ_2/ρ_1 and R. The actual growth-rate

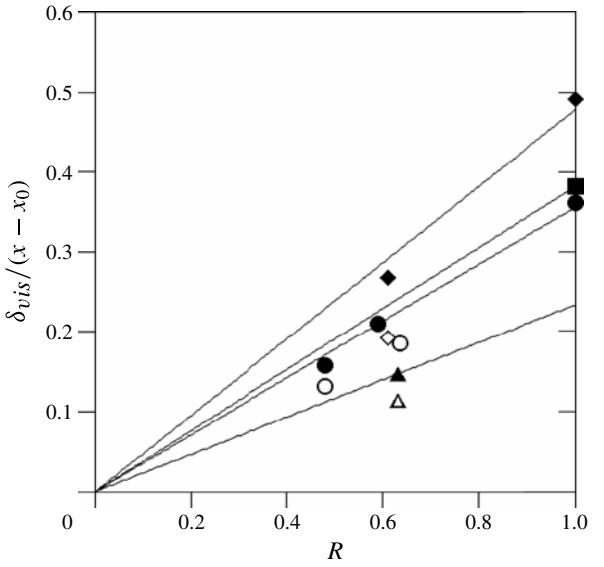

FIGURE 12. Visual-thickness growth rate versus non-dimensionalized velocity difference between free streams: $\rho_2/\rho_1 = 1.0$ (circles), 2.0 (square), 7.2 (diamonds) and 0.14 (triangles). Filled and unfilled symbols indicate organized and disorganized flow respectively. The reference lines are least-squares fits to the datum points for organized flow.

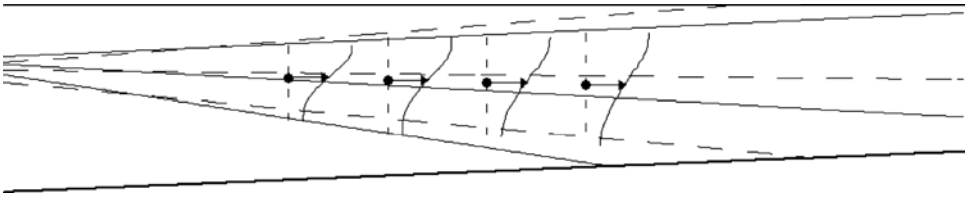

FIGURE 13. Orientations of self-similar mixing layer in its organized (continuous lines) and disorganized (broken lines) states for $U_1 = 31.8$ m s^{-1}, $U_2 = 7.3$ m s^{-1} and $\rho_2/\rho_1 = 1.0$ with walls of test section (bold lines) for reference. Also shown are four velocity profiles, the vector drawn on each profile indicating the transverse location at which the mean velocity was equal to the average of the free-stream values.

values measured here were slightly smaller than those measured by Brown & Roshko but these differences are not necessarily significant, given the imprecision of this type of measurement. The unfilled symbols in this figure show for comparison the visual growth rate of the wedge of turbulent fluid which formed the post-transition layer during the periods in which no procession of spanwise-coherent structures was present. In every case in which direct comparisons could be made this second growth rate was at least 10 % smaller than the first.

It was also observed that, during the periods in which the spanwise-coherent structures were absent, the whole of the mixing layer was shifted towards the faster stream. This is illustrated for one particular uniform-density case in figure 13 where the visual edges and centreline of the layer during the periods of organized and

disorganized flow are plotted to scale as straight lines extrapolated back towards the virtual origin with the walls of the test section for reference. This was the highest-growth-rate test run performed in the narrower build 1 test section and it can be seen that, with the lower wall angled upwards at the angle necessary to eliminate the average streamwise pressure gradient, the layer made contact with the lower wall when the structures were present but impinged instead on the upper wall when the structures were absent. Also plotted on this diagram are the measured mean velocity profiles at four different stations in the self-similar part of the flow, the arrowed vector drawn on each profile marking the location of the point at which the measured velocity was equal to the average of the free-stream values. These profiles will have included contributions from both flow states, weighted in proportion to their relative probabilities, and so it is not surprising to see that this mean vector lies between the two visual centrelines.

This change in the orientation of the mixing layer relative to the free streams implies that, in its two states (organized and disorganized), the layer entrained different relative proportions of the two free-stream fluids. An approximate measure of the two entrainment ratios can be obtained from the various flow angles using a variant of the method employed previously by Hermanson & Dimotakis (1989). This exploits the fact that, where the growth of the mixing layer is self-similar, the volumetric entrainment from each free stream can be evaluated directly from the magnitude of the free-stream vector and its angle to the edge of the layer.

To evaluate and compare these entrainment ratios in a consistent and non-arbitrary way, the free-stream velocities for each flow state must be projected onto a coordinate system which is based on the centreline of the mixing layer and thus rotated through the angle α_C relative to the fixed upper wall of the test section (figure 14*a*). With all rotations taken as positive in the anticlockwise direction, the angles of the free streams relative to the X axis are then

$$\alpha_1 = -\alpha_C \tag{3.10a}$$

$$\alpha_2 = -\alpha_C + \alpha_W \tag{3.10b}$$

where α_W is the angle of elevation of the hinged lower wall. The volumetric fluxes of the two fluids into unit span and unit length of the post-transition mixing layer are then given by

$$\dot{V}_1 = U_1 \left(\frac{\mathrm{d}\delta_{vis}/\mathrm{d}X}{2} \cos\alpha_1 - \sin\alpha_1 \right) \tag{3.11a}$$

$$\dot{V}_2 = U_2 \left(\frac{\mathrm{d}\delta_{vis}/\mathrm{d}X}{2} \cos\alpha_2 + \sin\alpha_2 \right) \tag{3.11b}$$

and the relative volumetric proportions of the two fluids entrained into the layer by the entrainment ratio

$$E_V = \frac{\dot{V}_1}{\dot{V}_2}. \tag{3.12}$$

In the case shown in figure 13, the resultant values of E_V for the layer in its organized and disorganized states are calculated to have been approximately 1.0 and 2.4, respectively.

These determinations are of limited accuracy because: (i) the experimental mixing layer did not actually grow in the assumed self-similar manner over the whole of its length; (ii) the values of $\dot{V}_1$ and $\dot{V}_2$ are very sensitive to even small errors in the

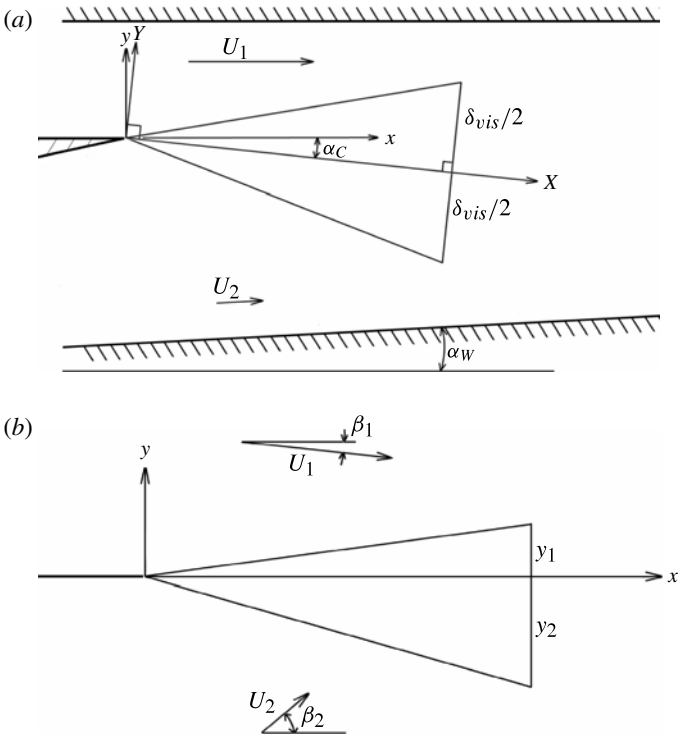

FIGURE 14. (*a*) Coordinate system for analysis of entrainment by experimental mixing layer. (*b*) Coordinate system for mixing-layer analysis of Abramovich.

angles α_1 and α_2. Small errors in these angles, as evaluated from (3.10), arise from neglect of the finite displacement thicknesses of the boundary layers growing on the walls of the test section. A more serious problem is that the adjustable lower wall was set at the angle which eliminated the time-averaged streamwise pressure gradient. It must be expected that the growth rate of the displacement thickness of the mixing layer ($=\tan\alpha_1 - \tan\alpha_2$) will have been different for the layer in its organized and disorganized states and that, because the layer was continually switching between these states, the wall angle set will have been incorrect to a greater or lesser extent for both of them.

A first test of the accuracy of these measured values of E_V is provided by the requirement for flow continuity. If an isothermal gaseous mixing layer grows in a steady self-similar manner over the whole of its length under conditions of uniform pressure, continuity requires that the integral volume flow within the layer through any plane normal to the X axis be equal to the total volumetric inflow from the free streams upstream of that plane. Thus, if the velocity fluctuations within the layer are completely random so that Reynolds averaging can be applied to the outflow from the control volume in figure 14(*a*),

$$\left(\dot{V}_1 + \dot{V}_2\right) X = \int_{-\delta_{vis}/2}^{\delta_{vis}/2} \bar{u}\,\mathrm{d}Y \tag{3.13}$$

where $\bar{u}\,(X, Y)$ represents the local mean velocity associated with the convection of the mixing-layer fluid parallel to the X axis. In the case of a uniform-density mixing layer

it is convenient to follow Abramovich (1963) and take Schlichting's formula

$$\frac{U_1 - \bar{u}}{U_1 - U_2} = \left(1 - \eta^{3/2}\right)^2 \tag{3.14}$$

as an approximation to the mean velocity profile $\bar{u}(\eta)$, where η is a dimensionless ordinate which increases linearly from 0 to 1 as Y increases from $-\delta_{vis}/2$ to $+\delta_{vis}/2$. In the particular case presented in figure 13 use of this profile to evaluate the right-hand side of (3.13) results in a continuity imbalance of just 6 %. This is reduced to ~4 % when a realistic correction is made to α_1 and α_2 for the displacement thicknesses of the wall boundary layers. This result suggests that the wall angle set in this experiment was close to that required to provide conditions of uniform shear for the self-similar part of the mixing layer in its disorganized state.

In the case of the organized post-transition mixing layer the continuity balance must in general be expressed in a form different form that of (3.13). As was shown in § 3.3, the flow within the layer is here organized into a procession of self-preserving coherent parcels of fluid (the vortex-like structures and the tongues of entrained fluid trapped between them) each of which occupies the whole of the layer's visual thickness and convects bodily along the X axis at the velocity U_C. The large-scale velocity fluctuations within the layer are therefore non-random and, measured in the Eulerian frame, the local mean velocity $\bar{u}$ includes non-zero contributions from the fluctuations associated with the rotations of the structures and the corresponding induced motions in the entrained fluid trapped between the rotating structures. But these fluctuations are functionally the largest scales in the turbulence spectrum and contribute nothing to the net transport of fluid in the X direction. To evaluate the net convection it is necessary to consider the Galilean transformation required to bring the coherent parcels of fluid to rest and replace (3.13) by the balance

$$\dot{V}_1 + \dot{V}_2 = U_C \frac{\mathrm{d}\delta_{vis}}{\mathrm{d}X} \tag{3.15}$$

with U_C given by (3.8). It is only where the density is uniform and the two halves of the measured mean velocity profile are near-antisymmetric that (3.13) and (3.15) become approximately equivalent.

In the particular case presented in figure 13 the right-hand side of (3.15) was greater than the left-hand side by some 37 % (reduced to ~34 % with corrections for the wall boundary layers), implying that a significantly larger wall angle than that actually set would have been needed to provide uniform shear for the self-similar part of this mixing layer in its organized state. As it was, there will have been an adverse pressure gradient within the relevant part of the test section during the periods of organized flow, causing both R and $\mathrm{d}\delta_{vis}/\mathrm{d}X$ to increase progressively with X.

Reference values of E_V for comparison with the two measured values given above can themselves be estimated only approximately at the present time. Brown (1974) has hypothesized, from theoretical consideration of the temporally evolving mixing layer formed between two counterflowing streams, that E_V for a mixing layer containing a row of spanwise-oriented vortices is approximately equal to $(\rho_2/\rho_1)^{1/2}$. This suggests a value very close to the measured value of ~1.0 for the uniform-density mixing layer of figure 13 in its organized state. However, numerous measurements of the composition of the mixed fluid formed within real spatially evolving mixing layers have shown that there is a definite bias, separate from any associated with the density ratio, towards entrainment from the faster stream. From consideration of the average streamwise increase in the size and spacing of the vortices, Dimotakis (1986) has

argued that the spatial bias factor can be written as

$$\Phi \approx 1 + 0.68R \tag{3.16}$$

and that a general expression for the entrainment ratio is therefore

$$E_V = \Phi \sqrt{\rho_2/\rho_1} \approx (1 + 0.68R) \sqrt{\rho_2/\rho_1}. \tag{3.17}$$

This suggests an E_V value of 1.43 for the conditions of figure 13. This is still reasonably close to the measured value, given that there was an adverse pressure gradient in the relevant part of the test section when the mixing layer was in its organized state.

A theoretical estimate of E_V for the mixing layer in its disorganized state is provided by the analytical solution of the governing continuity and momentum equations developed by Abramovich (1963) for the classical problem of a turbulent mixing layer between two infinite streams. Abramovich casts his analysis in x–y coordinates aligned with the splitter plate (figure 14*b*) and makes the usual assumption that there is no significant variation of static pressure within the flow. With this assumption the free streams must take up angles β_1 and β_2 to the x axis that are negative and positive, respectively. Rotations are again taken as positive in the anticlockwise direction and U_1 and U_2 again represent the free-stream vectors.

Continuity requires that the integral mass flow within the mixing layer through any plane normal to the x axis be equal to the total inflow from the free streams. Thus, in the case of uniform density,

$$U_1 (y_1 \cos\beta_1 - x \sin\beta_1) + U_2 (y_2 \cos\beta_2 + x \sin\beta_2) = \int_{-y_2}^{y_1} \bar{u}\, \mathrm{d}y \tag{3.18}$$

where $\bar{u}(x, y)$ is now the mean velocity parallel to the x axis. Once again $\bar{u}$ is approximated by Schlichting's formula which can here be written as

$$\frac{U_1 - \bar{u}}{U_1 \cos\beta_1 - U_2 \cos\beta_2} = \left[1 - \left(\frac{y - y_2}{\delta}\right)^{3/2}\right]^2 \tag{3.19}$$

where $\delta(x)$ is the finite thickness of the mixing layer defined by this velocity profile and taken to be the same as the visual thickness δ_{vis}. In the absence of pressure gradients and neglecting the second-order fluctuation correlation term, the corresponding balance of momentum in the x direction requires that

$$U_1^2 \cos\beta_1 (y_1 \cos\beta_1 - x \sin\beta_1) + U_2^2 \cos\beta_2 (y_2 \cos\beta_2 + x \sin\beta_2) = \int_{-y_2}^{y_1} \bar{u}\bar{u}\, \mathrm{d}y. \tag{3.20}$$

With δ/x supplied empirically, the balance of momentum in the y direction

$$U_1^2 \sin\beta_1 (y_1 \cos\beta_1 - x \sin\beta_1) + U_2^2 \sin\beta_2 (y_2 \cos\beta_2 + x \sin\beta_2) = 0 \tag{3.21}$$

then produces a closed system of equations which can be solved for β_1 and β_2. Projection of this solution onto the mixing-layer-centred X–Y coordinates used previously and use of (3.11) and (3.12) yielded an E_V value of 2.0 for the conditions of figure 13, to be compared with the measured value of ~2.4.

Despite the errors, assumptions and approximations in these various determinations, there is a good level of consistency between the measured and predicted values of E_V. Both confirm the direct evidence of the flow visualizations that, when the organization within the mixing layer breaks down, there is a significant change in the entrainment

ratio in favour of fluid from the faster stream. This in turn causes a significant change in the orientation of the mixing layer relative to the free streams. Although analysed in detail here for only a single set of flow conditions, similar effects of the flow state (organized or disorganized) on the entrainment ratio were seen when (3.10), (3.11) and (3.12) were applied to the flow visualizations produced for other velocity and density ratios.

As has been discussed elsewhere (Coats 1996), these effects of the large-scale organization on the entrainment ratio and orientation of the post-transition mixing layer can both be rationalized dynamically from further consideration of the streamwise momentum balance. Considering for simplicity the limiting single-stream case ($R = 1$), (3.20), in coordinates aligned with the fixed upper wall of the test section, reduces to

$$U_1^2 y_1 = \int_{-y_2}^{y_1} \bar{u}\bar{u}\,\mathrm{d}y. \tag{3.22}$$

If $\bar{u}(x, y)$ is approximated by Schlichting's formula, this yields $y_1 = 0.416\delta$ for the mixing layer in its disorganized state. If the mixing layer organizes itself into a procession of rotating coherent structures, however, the fluctuations associated with the rotations of the structures, whilst contributing to the measured mean velocity profile, do not contribute directly to the net flux of momentum out of the control volume to which (3.20) relates. By the same logic as was applied to the derivation of (3.15), if the structures occupy the full thickness of the layer and convect bodily in the x direction with velocity U_C, the balance of x-direction momentum instead becomes

$$U_1^2 y_1 = U_C^2 \delta \tag{3.23}$$

and, if $U_C = U_1/2$, y_1 becomes equal to 0.25δ. This represents a substantial displacement of the layer away from the moving stream. The change in the entrainment ratio then follows as a necessary consequence of the change of orientation.

4. Discussion

The present more rigorous and extensive experiments confirm the earlier unpublished findings of Pedley (1990) that, at the mixing transition, the mechanism by which the mixing layer grows changes fundamentally. In the pre-transition flow the spanwise-oriented vortices grow by the well-known process of vortex amalgamation, driven by the sequential excitation of the subharmonics of the fundamental Kelvin–Helmholtz instability. In the post-transition flow these subharmonics are no longer the agency of growth and instead the individual large structures (which are now turbulent vortex cores) undergo continuous linear growth between interactions. The interactions between neighbouring structures that occur in the post-transition flow are different in character from their pre-transition counterparts and occur as a consequence of the growth of the individual structures, not its cause.

It is surprising, in view of the large amount of work that has been done on this canonical flow, that this step change in the growth mechanism has escaped general recognition for so long and that it was not spotted in the years immediately following the publication of the seminal papers of Brown & Roshko (1974) and Winant & Browand (1974). The explanation can only be that, at the time when the growth mechanism of the mixing layer was the subject of intense debate, the existence of the mixing transition was itself unknown and the development of the mixing layer

towards a universal fully turbulent state was assumed to be continuous and a function simply of the local Reynolds number. There was therefore no reason to look for a step change in the growth mechanism at any particular point in the flow development. By the time that Breidenthal's (1981) paper had established the existence of this transition (Konrad's earlier thesis had remained unpublished) the growth mechanism was no longer being actively debated and interest was focused on the processes leading up to the transition and on the effects of the transition on the molecular-scale mixing within the flow.

Thus, in an early review paper, Roshko (1976) was able to present a sequence of images showing what were very clearly instability-driven vortex amalgamations occurring at very high Reynolds number as evidence supporting the idea that such amalgamations did in fact contribute to the self-similar growth of the fully developed flow. In the light of what is now known about the development of mixing layers from a laminar initial state it can be seen that the amalgamations in this image sequence (figure 3 of Roshko's paper) were actually occurring in the pre-transition part of the flow. Although the Reynolds numbers at which these amalgamations were occurring were as high as 7×10^4 (evaluated on the basis of the velocity difference across the mixing layer and the local visual thickness, as in the present work), the velocity of the faster stream in this experiment was quite modest, the boundary layer separating from the high-speed side of the splitter plate is unlikely to have been especially thin and it is not surprising to see the pre-transition part of the flow occupying a significant part of the available flow length. Indeed, the initial roll-up can be seen quite clearly in the image sequence and it appears that, as is entirely normal, it was the second amalgamation following the initial roll-up that triggered the transition.

Because it was assumed that the extent to which the flow was fully developed was simply a matter of the Reynolds number, there was also confusion at that time about the possible effect of density differences on the growth mechanism. In the same review paper, observing that the only progressive large-structure interactions evident in visualizations of mixing layers in which there was a large density difference between the two streams were of the sacrificial type described above in § 3.3, Roshko drew the tentative conclusion that it was the density difference that was responsible for this difference in the interaction pattern. But it is now obvious that these particular visualizations showed interactions of a different type because they were of the flow downstream of the mixing transition. As is shown clearly by our figures 9 and 10, there is, at the mixing transition, the same switch from growth by vortex amalgamation to continuous linear growth of the individual large structures (with occasional sacrificial interactions) irrespective of the density ratio between the free streams.

As was mentioned in § 1, the fact that many but not all of the vortex-like structures in mixing layers undergo continuous growth between interactions was first established by Hernan & Jimenez (1982) who subjected the large-structure evolution seen on one of the Caltech cine-film visualizations to a very detailed and fully software-driven statistical analysis. They did not distinguish in this analysis between the pre- and post-transition flows and it may reasonably be supposed that the structures that did and did not undergo the continuous growth were located downstream and upstream of the mixing transition, respectively. But the methodology they employed in their analysis also led them to less radical conclusions about the nature of the continuous growth than those reached by Pedley and ourselves. This requires more detailed consideration.

The analysis software used by Hernan & Jimenez fitted ellipses rather than circles to the braids visible in each side view (figure 8*b*) and took the area of each ellipse as

the measure of the size of the structure contained within it. Tracking of the structures from frame to frame showed that the areas of many of the individual ellipses increased in an approximately linear manner during the periods between the identifiable large-structure interactions. Hernan & Jimenez attributed this continuous growth of the individual ellipses to either the passive induction which continues after the saturation of an excited Kelvin–Helmholtz mode (Jimenez 1980) or outward turbulent diffusion from the vortex core (Moore & Saffman 1975). By this interpretation it is still the subharmonics of the fundamental Kelvin–Helmholtz instability that drive and sustain the self-similar growth of the mixing layer as a whole, by reconcentrating the vorticity at intervals and so reinvigorating the continuous growth of the individual structures in a cyclical manner.

Although superficially plausible, this interpretation of the cine-film evidence does not stand up when the two diameters of each ellipse are considered separately. As Hernan & Jimenez themselves reported, during the periods of continuous growth, the major axes of the ellipses defined by the curvature of the braids were in approximate alignment with the direction of flow and, with the structures all convecting at the same velocity, they will have remained near-constant in length between interactions. There can be little doubt, therefore, that the linear increase in the area of each ellipse measured by Hernan & Jimenez was actually the same linear increase in the length of its minor axis as was measured directly by ourselves and by Pedley. But as we commented earlier in § 3.3, this is incompatible with both passive induction by a vortex and radial turbulent diffusion because these processes would both require the minor diameter of each ellipse to increase as the square root of time.

To rationalize the observed continuous linear growth in diameter of the circular shapes tracked by ourselves and Pedley (or the equivalent continuous linear growth of the minor diameters of the elliptical ones tracked by Hernan & Jimenez) it is necessary to discard the widely made assumption that, in its organized state, the post-transition mixing layer can be analysed dynamically as a two-dimensional flow. As was discussed in § 1, the mixing transition does not occur until a system of secondary streamwise-oriented vortices has developed which loop backwards and forwards between the primary spanwise-oriented structures (Bernal & Roshko 1986). Moreover, it seems that this three-dimensional secondary structure persists in the post-transition flow, the spanwise spacing of the streamwise-oriented vortices adjusting itself in some way to maintain an approximately constant ratio to the streamwise spacing of the spanwise-oriented structures (Jimenez *et al.* 1985; Bernal & Roshko 1986; Bell & Mehta 1992). There thus exists in the post-transition layer a three-dimensional matrix of vortex lines which can be stretched and bent in complex ways, allowing the original spanwise-oriented vorticity to become intensified locally and reoriented in the streamwise and cross-stream directions or even reversed in sign. With these additional degrees of freedom in play we are no longer dealing with the simple redistribution of spanwise vorticity of constant circulation and two-dimensional analyses are inadequate. This will be demonstrated directly in Part 2 where it will be shown that three-dimensional simulations are needed to replicate numerically the continuous linear growth of the individual large structures seen in these experiments.

The other important findings from the present experiments concern the intermittent character of the large-scale organization in the post-transition mixing layer and the effect of the presence or absence of this organization on the similarity characteristics of the flow. When the large-scale organization disappears the growth rate of the mixing layer is reduced and there is a large change in its entrainment ratio with a corresponding change in its orientation relative to the free streams. It thus appears

that a turbulent mixing layer of any given velocity and density ratio can switch between two different self-similar states (organized and disorganized) and that the time-averaged similarity characteristics measured in different wind tunnels are likely to be made up of differently weighted contributions of both flow states. On the basis of the limited statistical evidence available it seems likely that all mixing layers relax to the disorganized state eventually but that the flow lengths necessary for this are very large. It may be conjectured that the well-documented persistence of the influence of the initial conditions discussed in § 1 is linked to the influence of the initial conditions on the rate at which the layer relaxes to a permanently disorganized state.

5. Conclusions

(i) Extensive new experiments have been carried out on single- and two-stream mixing layers developing naturally from laminar initial conditions. The experiments have covered wide ranges of free-stream velocity and density ratios and a wide range of mixing-layer Reynolds numbers. They differ from earlier published experiments of similar type in that the location of the mixing transition has been identified on a time-resolved basis from flow-visualization records and the growth of the cores of the vortex-like coherent structures has been measured directly.

(ii) It has been found that, at the instantaneous location of the mixing transition, there is, for all density ratios, a step change in the pattern of growth and interaction undergone by the large structures and consequently a change in the mechanism by which the mixing layer grows in thickness. Upstream of this transition the mixing layer grows by the well-known process of vortex amalgamation. Downstream of the transition the turbulent cores of the vortex-like structures individually occupy the full thickness of the mixing layer and grow continuously at a constant rate. When these structures are present it is the entrainment associated with their continuous linear growth that effects the self-similar growth of the mixing layer. The interactions which occur between the continuously growing structures in the post-transition flow are different in character from their pre-transition counterparts. They function simply to reduce at intervals the number of structures present and thus maintain a constant ratio between the average spacing of the structures and the local mixing-layer thickness.

(iii) The continuous linear growth displayed by the structures in the post-transition flow is incompatible with any simple two-dimensional induction or diffusion process and implies that there is a continuous three-dimensional redistribution of vorticity within the post-transition mixing layer when it is in this organized state.

(iv) It has been observed that the periods during which the post-transition part of the mixing layer comprises an organized procession of continuously growing structures are interrupted by periods during which no large-scale organization is evident downstream of the mixing transition. During these latter periods the self-similar growth rate of the mixing layer is reduced significantly and the orientation of the mixing layer relative to the fixed walls of the wind tunnel is changed, indicating a change in the ratio of the entrainment from the two streams. This change in the orientation of the mixing layer can be rationalized from consideration of the effect of the large-scale organization on the momentum balance within the flow.

Acknowledgements

The spectral measurements presented in this paper were made by Mr M. Evangelinakis. The authors also wish to acknowledge the very substantial inputs of Mr B. Chester, who made the wind tunnel used for this work, and of the other technical

staff who assisted with the experiments. The project was supported by EPSRC grant GR/J08096.

REFERENCES

ABRAMOVICH, G. N. 1963 *The Theory of Turbulent Jets*, pp. 149–162. MIT.

BATT, R. G. 1975 Some measurements on the effect of tripping the two-dimensional shear layer. *AIAA J.* **13**, 245–247.

BELL, J. H. & MEHTA, R. D. 1990 Development of a two-stream mixing layer from tripped and untripped boundary layers. *AIAA J.* **28**, 2034–2042.

BELL, J. H. & MEHTA, R. D. 1992 Measurements of the streamwise vortical structures in a plane mixing layer. *J. Fluid Mech.* **239**, 213–248.

BERNAL, L. P. & ROSHKO, A. 1986 Streamwise vortex structures in plane mixing layers. *J. Fluid Mech.* **170**, 499–525.

BRADSHAW, P. 1966 The effect of initial conditions on the development of a free shear layer. *J. Fluid Mech.* **26**, 225–236.

BREIDENTHAL, R. 1981 Structure in turbulent mixing layers and wakes using a chemical reaction. *J. Fluid Mech.* **109**, 1–24.

BROWAND, F. K. & LATIGO, B. O. 1979 Growth of the two-dimensional mixing layer from a turbulent and nonturbulent boundary layer. *Phys. Fluids* **22**, 1011–1019.

BROWAND, F. K. & TROUTT, T. R. 1985 The turbulent mixing layer: geometry of large vortices. *J. Fluid Mech.* **158**, 489–509.

BROWAND, F. K. & WEIDMAN, P. D. 1976 Large scales in the developing mixing layer. *J. Fluid Mech.* **76**, 127–144.

BROWN, G. L. 1974 The entrainment and large structure in turbulent mixing layers. In *Proceedings of Fifth Australasian Conference on Hydraulics and Fluid Dynamics, New Zealand, Christchurch*, pp. 352–359.

BROWN, G. L. & ROSHKO, A. 1974 On density effects and large structure in turbulent mixing layers. *J. Fluid Mech.* **64**, 775–816.

CHANDRSUDA, C., MEHTA, R. D., WEIR, A. D. & BRADSHAW, P. 1978 Effect of free stream turbulence on large structure in turbulent mixing layers. *J. Fluid Mech.* **85**, 693–704.

CLEMENS, N. T. & MUNGAL, M. G. 1995 Large-scale structure and entrainment in the supersonic mixing layer. *J. Fluid Mech.* **284**, 171–216.

COATS, C. M. 1996 Coherent structures in combustion. *Prog. Energy Combust. Sci.* **22**, 427–509.

COLES, D. 1981 Prospects for useful research on coherent structure in turbulent shear flow. *Proc. Indian Acad. Sci. (Eng. Sci.)* **4**, 111–127.

DAMMS, S. M. & KÜCHEMANN, D. 1974 On a vortex-sheet model for the mixing between two parallel streams. I. Description of the model and experimental evidence. *Proc. R. Soc. (Lond.)* A **339**, 451–461.

DIMOTAKIS, P. E. 1986 Two-dimensional shear-layer entrainment. *AIAA J.* **24**, 1791–1796.

DIMOTAKIS, P. E. 2000 The mixing transition in turbulent flows. *J. Fluid Mech.* **409**, 69–98.

DIMOTAKIS, P. E. & BROWN, G. L. 1976 The mixing layer at high Reynolds number: large-structure dynamics and entrainment. *J. Fluid Mech.* **78**, 535–560.

DZIOMBA, B. & FIEDLER, H. E. 1985 Effect of initial conditions on two-dimensional free shear layers. *J. Fluid Mech.* **152**, 419–442.

FIEDLER, H. E. & MENSING, P. 1985 The plane turbulent shear layer with periodic excitation. *J. Fluid Mech.* **150**, 281–309.

GEORGE, W. K. 1989 The self-preservation of turbulent flows and its relation to initial conditions and coherent structure. In *Advances in Turbulence* (ed. R. Arndt & W. K. George), pp. 39–73. Hemisphere.

HERMANSON, J. C. & DIMOTAKIS, P. E. 1989 Effects of heat release in a turbulent, reacting shear layer. *J. Fluid Mech.* **199**, 333–375.

HERNAN, M. A. & JIMENEZ, J. 1982 Computer analysis of a high-speed film of a plane turbulent mixing layer. *J. Fluid Mech.* **119**, 323–345.

HO, C.-M. & HUANG, L.-S. 1982 Subharmonics and vortex merging in mixing layers. *J. Fluid Mech.* **119**, 443–473.

HUANG, L.-S. & HO, C.-M. 1990 Small-scale transition in a plane mixing layer. *J. Fluid Mech.* **210**, 475–500.

HUSSAIN, A. K. M. F. & ZAMAN, K. B. M. Q. 1985 An experimental study of organised motions in the turbulent plane mixing layer. *J. Fluid Mech.* **159**, 85–104.

JIMENEZ, J. 1980 On the visual growth of a turbulent mixing layer. *J. Fluid Mech.* **96**, 447–460.

JIMENEZ, J. 1983 A spanwise structure in the plane shear layer. *J. Fluid Mech.* **132**, 319–336.

JIMENEZ, J., COGOLLOS, M. & BERNAL, L. P. 1985 A perspective view of the plane mixing layer. *J. Fluid Mech.* **152**, 125–143.

KARASSO, P. S. & MUNGAL, M. G. 1996 Scalar mixing and reaction in plane liquid shear layers. *J. Fluid Mech.* **323**, 23–63.

KOLMOGOROV, A. N. 1941 The local structure of turbulence in incompressible viscous fluid for very large Reynolds numbers. *C. R. (Dokl.) Acad. Sci. URSS* **30**, 301–305 Reprinted as *Proc. R. Soc. (Lond.) A* **434**, 9–13, 1991.

KONRAD, J. H. 1976 An experimental investigation of mixing in two-dimensional turbulent shear flows with applications to diffusion-limited chemical reactions. PhD thesis, California Institute of Technology (Issued as Project SQUID Tech. Rep. CIT-8-PU).

KOOCHESFAHANI, M. M., CATHERASOO, C. J., DIMOTAKIS, P. E., GHARIB, M. & LANG, D. B. 1979 Two-point LDV measurements in a plane mixing layer. *AIAA J.* **17**, 1347–1351.

KOOCHESFAHANI, M. M. & DIMOTAKIS, P. E. 1986 Mixing and chemical reactions in a turbulent liquid mixing layer. *J. Fluid Mech.* **170**, 83–112.

LASHERAS, J. C. & CHOI, H. 1988 Three-dimensional instability of a plane free shear layer: an experimental study of the formation and evolution of streamwise vortices. *J. Fluid Mech.* **189**, 53–86.

LASHERAS, J. C., CHO, J. S. & MAXWORTHY, T. 1986 On the origin and evolution of streamwise vortical structures in a plane, free shear layer. *J. Fluid Mech.* **172**, 231–258.

LIEPMAN, H. W. & LAUFER, J. 1947 Investigation of free turbulent mixing. NACA Tech. Note 1257.

LIN, S. J. & CORCOS, G. M. 1984 The mixing layer: deterministic models of a turbulent flow. Part 3. The effect of plane strain on the dynamics of streamwise vortices. *J. Fluid Mech.* **141**, 139–178.

MEYER, T. R., DUTTON, J. C. & LUCHT, R. P. 2006 Coherent structures and turbulent molecular mixing in gaseous planar shear layers. *J. Fluid Mech.* **558**, 179–205.

MICHALKE, A. 1965 Vortex formation in a free boundary layer according to stability theory. *J. Fluid Mech.* **22**, 371–383.

MICHALKE, A. 1971 Der Einfluß variabler Dichte auf die Instabilität einer freien Scherschicht. *Ing.-Arch.* **40**, 29–39.

MONKEWITZ, P. A. & HUERRE, P. 1982 Influence of the velocity ratio on the spatial instability of mixing layers. *Phys. Fluids* **25**, 1137–1143.

MOORE, D. W. & SAFFMAN, P. G. 1975 The density of organised vortices in a turbulent mixing layer. *J. Fluid Mech.* **69**, 465–473.

MOSER, R. D. & ROGERS, M. M. 1991 Mixing transition and the cascade to small scales in a plane mixing layer. *Phys. Fluids* A **3**, 1128–1134.

MOSER, R. D. & ROGERS, M. M. 1993 The three-dimensional evolution of a plane mixing layer: pairing and transition to turbulence. *J. Fluid Mech.* **247**, 275–320.

MUNGAL, M. G. & DIMOTAKIS, P. E. 1984 Mixing and combustion with low heat release in a turbulent mixing layer. *J. Fluid Mech.* **148**, 349–382.

MUNGAL, M. G., HERMANSON, J. C. & DIMOTAKIS, P. E. 1985 Reynolds number effects on mixing and combustion in a reacting shear layer. *AIAA J.* **23**, 1418–1423.

NYGAARD, K. J. & GLEZER, A. 1991 Evolution of streamwise vortices and generation of small-scale motion in a plane mixing layer. *J. Fluid Mech.* **231**, 257–301.

OSTER, D. & WYGNANSKI, I. 1982 The forced mixing layer between parallel streams. *J. Fluid Mech.* **123**, 91–130.

OSTER, D., WYGNANSKI, I. & FIEDLER, H. E. 1977 Some preliminary observations on the effect of initial conditions on the structure of the two-dimensional turbulent mixing layer. In *Turbulence in Internal Flows* (ed. S. N. B. Murthy), pp. 67–87. Hemisphere.

PEDLEY, T. J. 1990 An experimental investigation into coherent structures in free shear layer flows. PhD thesis, University of Leeds.

ROGERS, M. M. & MOSER, R. D. 1992 The three-dimensional evolution of a plane mixing layer: the Kelvin–Helmholz rollup. *J. Fluid Mech.* **243**, 183–226.

ROSHKO, A. 1976 Structure of turbulent shear flows: a new look. *AIAA J.* **14**, 1349–1357.

SLESSOR, M. D., BOND, C. L. & DIMOTAKIS, P. E. 1998 Turbulent shear-layer mixing at high Reynolds numbers: effects of inflow conditions. *J. Fluid Mech.* **376**, 115–138.

TOWNSEND, A. A. 1976 *The Structure of Turbulent Shear Flows*, 2nd edn. p. 196. Cambridge University Press.

WILKE, C. R. 1950 A viscosity equation for gas mixtures. *J. Chem. Phys.* **18**, 517–519.

WINANT, C. D. & BROWAND, F. K. 1974 Vortex pairing: the mechanism of turbulent mixing-layer growth at moderate Reynolds number. *J. Fluid Mech.* **63**, 237–255.

WOOD, D. H. & BRADSHAW, P. 1982 A turbulent mixing layer constrained by a solid surface. Part 1. Measurements before reaching the surface. *J. Fluid Mech.* **122**, 57–89.

WYGNANSKI, I. & FIEDLER, H. E. 1970 The two-dimensional mixing region. *J. Fluid Mech.* **41**, 327–361.